Modeling and Study of Nano-plasmonic Couplers of Different Shapes with Analytical Assessment Employing GaAs

by

Sheikh Montasir Mahbub (152415)

Nowshed Al Nur Hridoy (152432)

Anas Mahmood (152433)

Md. Sami Imtiaz (152434)

A Thesis Submitted to the Academic Faculty in Partial Fulfillment of the Requirements for the Degree of

BACHELOR OF SCIENCE

IN

ELECTRICAL AND ELECTRONIC ENGINEERING

Department of Electrical and Electronic Engineering
Islamic University of Technology (IUT)
Board Bazar, Gazipur-1704, Bangladesh.

Declaration of Authorship

We, Sheikh Montasir Mahbub, Nowshed Al Nur Hridoy, Anas Mahmood and Md. Sami Imtiaz declare the name of this dissertation, ‘Modeling and Study of Nano-plasmonic Couplers of Different Shapes with Analytical Assessment Employing GaAs’ and the works demonstrated in it are our own. We confirm that:

- This work has been presented for the purpose of the Bachelor of Science in Electrical and Electronic Engineering degree at this university.
- No section of this dissertation was submitted to receive any degree anywhere else.
- Furthermore, we specifically identified the references wherever we consulted other people's published work.

Submitted By:

_____

Sheikh Montasir Mahbub, 152415

_____

Nowshed Al Nur Hridoy, 152432

_____

Anas Mahmood, 152433

_____

Md. Sami Imtiaz, 152434

Approved By:

_____

Dr. Rakibul Hasan Sagor

Thesis Supervisor,

Assistant Professor,

Department of Electrical and Electronic Engineering,

Islamic University of Technology.

_____

Prof. Dr. Md. Ruhul Amin

Head of the Department,

Department of Electrical and Electronic Engineering,

Islamic University of Technology.

Abstract

One of the major advantages offered by the plasmonic devices is its ability to overcome diffraction limit of light that emerges due to miniaturization of the devices.

In order to serve this purpose plasmonic couplers of different shapes have been proposed. The proposed couplers consist of two types of waveguides; they are- Dielectric waveguide and MDM (Metal-Dielectric-Metal) waveguide. While designing the dielectric waveguide GaAs has been chosen as the key material. In MDM waveguide silver has been chosen as metal and air as dielectric. After designing the basic structures, different physical parameters were varied to optimize the performance of them. The performance of the proposed devices has been analyzed in terms of reflectance, admittance and transmitted energy.

Here, the performance deviation was ascertained varying the wavelength of the applied signal. Alternating the dimensions of the proposed nano-plasmonic coupling device, coupling efficiency, reflection coefficient and absorption coefficient were computed. Finally, novel architectures have been achieved which provides us the maximum efficiency.

Acknowledgements

First and foremost, we offer gratitude to the Almighty Allah (SWT) for blessing us with the capability to do this work.

We are grateful to our research supervisor, Dr. Rakibul Hasan Sagor, for the support and guidance throughout our research at Islamic University of Technology (IUT). He arranged a nice research environment where our ideas could thrive without any constraints. For all of his efforts as our true mentor, we express our heartfelt gratitude to him.

We would like to thank all the faculty members of the department of EEE, IUT for their inspiration and help.

And last but not the least we are thankful to our family and well-wishers for their support and inspiration. Without them it would never have been possible for us to make it this far.

Table of Contents

List of Figures

List of Tables

Chapter 1

Introduction

Electronics circuit works on the basis of transportation and storage of electron. Thanks to the use of scaled down transistors and electronic circuitries, the processing speed of modern microprocessors increased drastically. But in recent years, the annual rise in microprocessor clock speed has stagnated. This is due to the fact that RC delay increases with scaling down of electronic interconnects[1].

Through the implementation of optical communication systems based on optical fibers and photonics circuits, photonics offers a solution to this problem effectively. In comparison to system based on electronics, systems based on photonics such as fiber optic cable can transmit data much faster than electronic devices. However, they cannot be scaled down like electronic chips due to the diffraction limit of electromagnetic waves.

In order to provide a solution to this problem of size-compatibility, it is wise to use the surface plasmon based circuits which offers the astonishing possibility to combine electronics and photonics at the nanoscale. Surface plasmon-based photonics or plasmonics can solve the problems that arise from the dimensional mismatch of photonic and electronic devices. Surface plasmons (SP) are electromagnetic waves that propagate along the planar interface between a metal and dielectric medium due to the coherent oscillations of delocalized electrons[2]. SPPs have the potential to transcend diffraction limit[3]. Plasmonic waveguides based on metal-dielectric-metal (MDM) structure have the ability to deliver nanoscale light containment and direct optical modes of subwavelength i.e. surface Plasmon polaritons (SPPs)[4]. These characteristics of plasmonics waveguides make them the ideal linkage between photonic and electronic devices

1.1 Overview of Surface-Plasmon-Polariton

Surface plasmons (SP) are electromagnetic waves that propagate along the planar interface between a metal and dielectric medium due to the coherent oscillations of delocalized electrons. Such electromagnetic surface waves are generated due to the coupling of the electromagnetic fields to oscillations of the conductor's electron plasma.

SPPs are propagating solutions of Maxwell's equations at the interface between a dielectric and a metal, which are bound to that interface. They are the resonant interaction between a light wave and oscillations of the free electrons at the metal interface and have an evanescent tail into both the metal and the dielectric. The dispersion of SPPs on a smooth metal surface is given by,

$$k_x = k_o \sqrt{\frac{\epsilon_d \epsilon_m}{(\epsilon_d + \epsilon_m)}}, \tag{1.1}$$

where, $k_0 = \frac{\omega}{c}$ is the free-space wave vector. On a flat interface between dielectric and metal half-spaces with dielectric constants ε_d and ε_m, respectively, SPPs are transverse magnetic (TM) plane waves propagating along the interface. Assuming the interface is normal to z and the SPPs propagate along the x direction, the SPP wave vector k_x is related to the optical frequency through the dispersion relation. We take ω to be real and allow k_x to be complex, since our main interest is in stationary monochromatic SPP fields in a finite area. The details of SPP has been discussed in Chapter 3.

1.2 Background History

Plasmonics might be a modern concept but the photon interaction with the surface charges is not. It has been acknowledged by Joachim Krenn from the University of Graz, Austria that people were formulating ideas over 100 years which still connects to the researchers to this day. [5]

Moreover, the coupling of light to the surface charges has been exercised for several hundred years. Since science was still at a developing phase during that time, there remains a possibility of incorrect crediting to some cases of plasmonics. It is learnt that Maxwell, Garnett and others are among the pioneers to early research works during 1904. Since, there have been revival periods in the field every ten years or so. There were however mentionable developments in the 1980s and 1990s that accelerated the modern renaissance of plasmonics. By around 2001 there had been a fivefold increase in manuscript since 1990, which improved another five times by the year 2011.

In recent years, plasmonics has arguably become the most populated research field in optics. A principal characteristic of plasmonics is the probability of increasing electromagnetic field intensity locally. This allows significant optical nonlinear effects in metal inclusive systems, like metamaterials. Martti Kauranen and Anatoly Zayats demonstrated the topic of nonlinear effects in plasmonic structures and presentended an overview of applications and limitations4. In addition, Vasily Temnov covered the opportunities offered by surface plasmons in devices utilizing the amalgamation of magnetic, acoustic and ultrafast effects[6].

Nanofabricated structures using SPPs show potential for modeling and regulating propagation of light in matter. Generally, SPPs can be used to direct light effectively in nanometer-scale regions, resulting in specific modification of the resonance frequency dispersion properties (for example, significantly reducing the wavelength of light and the rate of light pulses), as well as field modifications appropriate for close interactions with nonlinear materials. The resulting increased sensitivity of light to external parameters (e.g. an applied electrical field or dielectric constant of an adsorbed molecular layer) shows potential for sensing and shifting applications.

Research currentlyfocuses on the structure, manufacturing, and experimental characterizatio n of modern communication components based on nanoscale plasmonic effects. There is frequent use of the excitation of SPPs in an experimental approach known as surface Plasmon resonance (SPR). In SPR, the maximum excitation of surface plasmons is defined as a function of the angle of incident, wavelength or phase by measuring the reflected power from a prism coupler. This technique can be used to observe nanometer changes in thickness, fluctuations in density, or adsorption by molecules.

The implementation of surface plasmon based circuits, including both SPPs and localized plasmon resonances can be an effective way to mitigate the size limitation issue of photonic circuits in the operation of high-performance data processing nano devices. However, in case of metal-dielectric-metal configuration of plasmonic waveguide, the propagation length of SPP is limited due to its high propagation loss at the surface of the metal, which is significantly more than the losses occurring due to disorders that are related to fabrications. Using both dielectric and plasmonic waveguide on the same chip can resolve this issue.
The dielectric waveguide will carry the elementary optical mode,while the plasmonic wavegui de addresses the problem of the subwavelength scale.
This requires the need to couple optical modes efficiently from the dielectric waveguide to the plasmonic waveguide.The design of efficient nanoplasmonic couplers with various materials a nd structures can therefore be a visionary step in miniaturizing integrated photonic devices.

G. Veronis et. al [7][8] proposed a coupler with multi-section tapers. P. Ginzburg et al [9] reported a $\lambda/4$ coupler to couple optical modes from a 0.5m to 50nm wide plasmonic waveguide. D. Pile et al. [10][11] presented an adiabatic and a non-adiabatic tapered plasmonic coupler. R. Wahsheh et al.[12][13] reported an analysis on nano plasmonic air-slot coupler and its fabrication steps.

1.3 Thesis Objective

The prime objective of the thesis is to design and analyze efficient nano-plasmonic couplers of different shapes. Here we have proposed two different structures of nano-plasmonic waveguide deploying GaAs and analyzed their performance parameters. In terms of results (transmittance, absorbance, reflectance) obtained from the simulations indicate the verification of the system. However, more specifically, the objectives are-

- to develop a model based on the FDTD method where we can run simulations in order to observe different performance parameters,
- to obtain validity of the designed nano structures by measuring the energy through different ports,
- to propose an efficient structure from the obtained results and discuss the potential applications.

1.4 Thesis Organization

The thesis has been arranged in the following way:

- In Chapter 2, the basic theory of EM Wave has been described. This chapter introduces the fundamental knowledge and necessary mathematical formulations of EM Wave and Maxwell's equation.
- In Chapter 3, the concept and mathematical formulation of Surface Plasmon Polariton (SPP) has been described.
- Since we have developed our simulation model based on Numerical Analysis Method. These methods are briefly described in Chapter 4.
- In chapter 5, design and analysis of our proposed nano-plasmonic couplers are discussed.

Chapter 2

Basics of Electromagnetics

Plasmonics works as a bridge between photonics and electronics. This field basically deals with light which is an electromagnetic wave. Maxwell came up with a set of differential equations in 1873 to explain the propagation of electromagnetic waves which is considered as the base of electromagnetics.

2.1 Maxwell's Equation

Maxwell's equations are a set of differential equations, and they are the base of all the studies and research work done on the field of electromagnetics.

These equations are an assembled version of Gauss's law, Gauss's law for magnetism, Faraday's law and Ampere's law. The integral form of Maxwell's equation can be summarized[14] as,

$$\oint_s \mathbf{D}.\,\mathrm{dS} = \int_v \boldsymbol{\rho}_v \,.dv, \tag{2.1}$$

$$\oint_s \mathbf{B}.\,\mathrm{dS} = 0, \tag{2.2}$$

$$\oint_L \mathbf{E}.\,\mathrm{dl} = -\frac{\partial}{\partial \mathrm{t}} \int_s \mathbf{B}\,.\,\mathrm{dS}, \tag{2.3}$$

$$\oint_L \mathbf{H}.\,\mathrm{dl} = \int_s \left(\mathbf{J} + \frac{\partial \mathbf{D}}{\partial \mathrm{t}}\right).\,\mathrm{dS}. \tag{2.4}$$

And the general form of time varying Maxwell's equation in differential form can be written as,

$$\nabla \times \mathbf{E} = -\frac{\partial \mathbf{B}}{\partial \mathrm{t}} - \mathbf{M}, \tag{2.5}$$

$$\nabla \times \mathbf{H} = \mathbf{J} + \frac{\partial \mathbf{D}}{\partial \mathrm{t}}, \tag{2.6}$$

$$\nabla.\,\mathbf{D} = \boldsymbol{\rho}, \tag{2.7}$$

$$\nabla . \mathbf{B} = 0, \tag{2.8}$$

where,

E is the electric field, in volts per meter (V/m).

H is the magnetic field, in amperes per meter (A/m).

D is the electric flux density, in coulombs per meter squared (C/m^2)

B is the magnetic flux density, in Weber's per meter squared (Wb/m^2)

M is the (fictitious) magnetic current density, in volts per meter (V/m^2).

J is the electric current density, in amperes per meter squared (A/m^2).

ρ is the electric charge density, in coulombs per meter cubed (C/m^3).

In free-space, the electric and magnetic field intensities and flux densities are related in this way,

$$\mathbf{B} = \mu_0 \mathbf{H} , \tag{2.9}$$

$$\mathbf{D} = \varepsilon_0 \mathbf{E} . \tag{2.10}$$

Assuming an $e^{j\omega t}$ time dependence, the time derivatives in (2.5)– (2.8) can be replaced with jω. Maxwell's equations in phasor form become,

$$\nabla \times \mathbf{E} = -\mathrm{j}\omega \mathbf{B} - \mathbf{M}, \tag{2.11}$$

$$\nabla \times \mathbf{H} = \mathbf{J} + \mathrm{j}\omega \mathbf{D}, \tag{2.12}$$

$$\nabla . \mathbf{D} = \boldsymbol{\rho}, \tag{2.13}$$

$$\nabla . \mathbf{B} = 0. \tag{2.14}$$

The Fourier transform can be used to convert a solution to Maxwell's equations for an arbitrary frequency ω into a solution for arbitrary time dependence.[15]

2.2 The Helmholtz Equation

Helmholtz equation is named after Herman von Helmholtz, a German physician. The Helmholtz equation is a linear partial differential equation,

$$(\nabla^2 + \mathrm{K}^2)\mathrm{A} = 0, \tag{2.15}$$

where,

∇^2 is the Laplacian,
k is wave number ,
and A is the amplitude of the wave[16].
This equation is applied to shape Maxwell's equation in a source-free, linear, isotropic, homogeneous region, Maxwell's curl equations in phasor form are,

$$\nabla \times \mathbf{E} = -\mathrm{j}\omega\mu\mathbf{H}, \tag{2.16}$$

$$\nabla \times \mathbf{H} = \mathrm{j}\omega\epsilon\mathbf{E}, \tag{2.17}$$

and constitute two equations for the two unknowns, **E** and **H**. As such, they can be solved for either **E** or **H**. Taking the curl of (2.11) and using (2.12) gives,

$$\nabla \times \nabla \times \mathbf{E} = -\mathrm{j}\omega\mu\nabla \times \mathbf{H} = \omega^2\mu\epsilon\mathbf{E}, \tag{2.18}$$

which is an equation for **E.**

This result can be simplified through the use of vector identity $\nabla\times\nabla\times \mathbf{E} = \nabla.(\nabla.\mathbf{E}) - \nabla^2\mathbf{E}$, which is valid for the rectangular components of an arbitrary vector **E**, then,

$$\nabla^2\mathbf{E} + \omega^2\mu\varepsilon\mathbf{E} = 0, \tag{2.19}$$

because $\nabla \cdot \mathbf{E} = 0$ in a source-free region. Equation (2.14) is the Helmholtz equation, for **E**. Similar equation for **H** can be derived in the same manner,

$$\nabla^2\mathbf{H} + \omega^2\mu\varepsilon\,\mathbf{H} = 0. \tag{2.20}$$

A constant $k = \omega\sqrt{\mu\varepsilon}$ is defined and called the propagation constant (which is also known as wave number), of the medium; its units are 1/m $.

2.3 General Plane Wave Solutions

Finally, the wave equation for **E** in free space can be written as,

$$\nabla^2\mathbf{E} + k^2\mathbf{E} = \frac{\partial^2\mathbf{E}}{\partial x^2} + \frac{\partial^2\mathbf{E}}{\partial y^2} + \frac{\partial^2\mathbf{E}}{\partial z^2} + k^2\mathbf{E} = 0. \quad (2.21)$$

In similar way, the wave equation for **H** in free space can be written as,

$$\nabla^2\mathbf{H} + k^2\mathbf{H} = \frac{\partial^2\mathbf{H}}{\partial x^2} + \frac{\partial^2\mathbf{H}}{\partial y^2} + \frac{\partial^2\mathbf{H}}{\partial z^2} + k^2\mathbf{H} = 0. \quad (2.22)$$

Chapter 3

Surface Plasmon Polariton

Surface plasmon polaritons are electrical excitations that move in the perpendicular direction of the interface between a dielectric and a conductor. Through the coupling of electromagnetic fields to oscillations of the electron plasma of the conductor, these electromagnetic surface waves are created.

3.1 The Wave Equation

To observe the physical properties of surface plasmon polaritons (SPPs), Maxwell's equations (2.5), (2.6), (2.7), (2.8) are needed to be implemented to the flat interface between a conductor and a dielectric. To order to present this topic as clearly as possible, it is desirable to cast the equations first in a general form applicable to the guiding of electromagnetic waves, the wave equation.

Without the external charge and the current densities, the curl equations (2.5, 2.6) can be combined to yield,

$$\nabla \times \nabla \times \mathbf{E} = -\mu_o{}^2 \frac{\partial^2 \mathbf{B}}{\partial t^2}. \tag{3.1}$$

Using $\nabla \times \nabla \times \mathbf{E} \equiv \nabla (\nabla \cdot \mathbf{E}) - \nabla^2 \mathbf{E}$ as well as $\nabla \cdot (\varepsilon \mathbf{E}) \equiv \mathbf{E} \cdot \nabla\varepsilon + \varepsilon \nabla \cdot \mathbf{E}$, and considering the lack of $\nabla \cdot \mathbf{D} = 0$, (3.1) can be rewritten as,

$$\nabla\left(-\frac{1}{\epsilon}\mathbf{E}.\nabla\epsilon\right) - \nabla^2\mathbf{E} = -\mu_o\epsilon_o\epsilon\frac{\partial^2\mathbf{E}}{\partial t^2}. \tag{3.2}$$

For negligible dielectric profile variation $\varepsilon = \varepsilon(\mathbf{r})$ over distances on the order of one optical wavelength, (3.2) Simplifies the basic formula of the theory of electromagnetic waves,

$$\nabla^2\mathbf{E} - \frac{\epsilon}{c^2}\frac{\partial^2\mathbf{E}}{\partial t^2} = 0\ . \tag{3.3}$$

In practice, this equation has to be solved individually in regions of constant ε and the solutions obtained have to be matched according to the appropriate boundary conditions. To cast (3.3) appropriate for the description of confined waves, we proceed in two steps. First, we assume in all generality a harmonic time dependence $\mathbf{E}(\mathbf{r}, t) = \mathbf{E}(\mathbf{r})\, e^{-i\omega t}$ of the electric field. Inserted into (3.3), this yield,

$$\nabla^2\mathbf{E} - k_o{}^2\epsilon\mathbf{E} = 0\ . \tag{3.4}$$

where, $k_o = \frac{\omega}{c}$ is the propagating wave vector in the vacuum. Equation (3.4) is called Helmholtz equation.

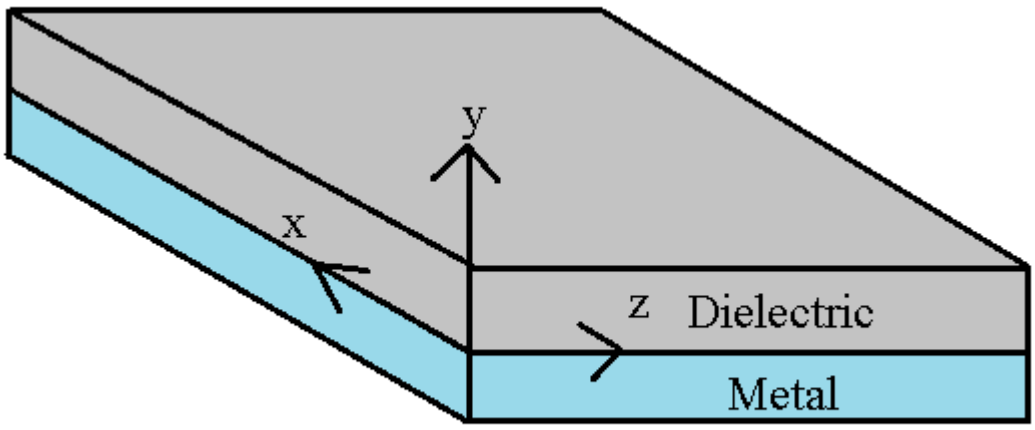

Fig. 3.1: Typical geometry of the planar waveguide. The waves propagate in a cartesian coordination system along the x-direction.

For simplicity let us assume that the wave propagation is along the x-direction of the Cartesian coordinate system and that there is no spatial variation in the y-direction. We can therefore write,

$$\mathbf{E}(x, y, z) = \mathbf{E}(z)e^{j\beta z}. \tag{3.5}$$

Where, $\beta = K_x$ which is known as the propagation constant.

Now, inserting the value of **E**, the wave equation will be,

$$\frac{\partial^2 \mathbf{E}(z)}{\partial z^2} + (K_0^2\varepsilon - \beta^2)\mathbf{E} = 0. \tag{3.6}$$

In the same way, we can determine equation for the magnetic field **H**. The field **E** and **H** can be decomposed in cartesian co-ordinate system as,

$$\mathbf{E} = \mathbf{E}_x.\vec{a}_x + \mathbf{E}_y.\vec{a}_y + \mathbf{E}_z.\vec{a}_z, \tag{3.7}$$

$$\mathbf{H} = \mathbf{H}_x.\vec{a}_x + \mathbf{H}_y.\vec{a}_y + \mathbf{H}_z.\vec{a}_z. \tag{3.8}$$

For Harmonic time dependence $\frac{\partial}{\partial t} = -j\omega$ and by solving the Ampere's law and Faraday's law, we get,

$$\frac{\partial \mathbf{E}_z}{\partial y} - \frac{\partial \mathbf{E}_y}{\partial z} = j\omega\mu_0 \mathbf{H}_x, \tag{3.9}$$

$$\frac{\partial \mathbf{E}_x}{\partial z} - \frac{\partial \mathbf{E}_z}{\partial x} = j\omega\mu_0 \mathbf{H}_y, \quad , \tag{3.10}$$

$$\frac{\partial \mathbf{E}_y}{\partial x} - \frac{\partial \mathbf{E}_x}{\partial y} = j\omega\mu_0 \mathbf{H}_z, \tag{3.11}$$

$$\frac{\partial \mathbf{H}_z}{\partial y} - \frac{\partial \mathbf{H}_y}{\partial z} = j\omega\varepsilon_0 \varepsilon\mathbf{E}_x, \tag{3.12}$$

$$\frac{\partial \mathbf{H}_x}{\partial z} - \frac{\partial \mathbf{H}_z}{\partial x} = j\omega\varepsilon_0 \varepsilon\mathbf{E}_y, \tag{3.13}$$

$$\frac{\partial \mathbf{H}_y}{\partial x} - \frac{\partial \mathbf{H}_x}{\partial y} = j\omega\varepsilon_0 \varepsilon\mathbf{E}_z. \tag{3.14}$$

As the propagation is in x-direction in the form of $e^{j\beta x}$ which supersedes $\frac{\partial}{\partial x} = -j\beta$.

The homogeneity in y- direction make $\frac{\partial}{\partial y} = 0$. So, it will modify the equation as,

$$-\frac{\partial \mathbf{E}_y}{\partial z} = j\omega\mu_0 \mathbf{H}_x, \tag{3.15}$$

$$\frac{\partial \mathbf{E}_x}{\partial z} - j\beta \mathbf{E}_z = j\omega\mu_0 \mathbf{H}_y, \tag{3.16}$$

$$j\beta \mathbf{E}_y = j\omega\mu_0 \mathbf{H}_z, \tag{3.17}$$

$$\frac{\partial \mathbf{H}_y}{\partial z} = j\omega\varepsilon_0 \varepsilon \mathbf{E}_x, \tag{3.18}$$

$$\frac{\partial \mathbf{H}_x}{\partial z} - j\beta \mathbf{H}_z = j\omega\varepsilon_0 \varepsilon \mathbf{E}_y, \tag{3.19}$$

$$j\beta \mathbf{H}_y = j\omega\varepsilon_0 \varepsilon \mathbf{E}_z. \tag{3.20}$$

The solution of the above equation can be characterized by two sets of solution with the polarized characteristics which are, Transverse Electric (TE) modes and Transverse Magnetic (TM) modes. The equations belong to Transverse Magnetic modes are,

$$\mathbf{E}_x = -j\frac{1}{\omega\varepsilon_0 \varepsilon}\frac{\partial \mathbf{H}_y}{\partial z}, \tag{3.21}$$

$$\mathbf{E}_z = -\beta\frac{1}{\omega\varepsilon_0 \varepsilon}\mathbf{H}_y. \tag{3.22}$$

Therefore, The TM polarized wave Equation will be,

$$\frac{\partial^2 \mathbf{H}_y}{\partial z^2} + (K_0^2\varepsilon - \beta^2)\mathbf{H}_y = 0. \tag{3.23}$$

Similarly, the TE polarized equations will be,

$$\mathbf{H}_x = j\frac{1}{\omega\mu_0}\frac{\partial \mathbf{E}_y}{\partial z}, \tag{3.24}$$

$$\mathbf{H}_z = \beta\frac{1}{\omega\mu_0}\mathbf{E}_y. \tag{3.25}$$

And the corresponding TE wave equation will be,

$$\frac{\partial^2 \mathbf{E}_y}{\partial z^2} + (K_0^2 \varepsilon - \beta^2)\mathbf{E}_y = 0. \tag{3.26}$$

3.2 SPP at Single Interface

The simplest configuration of SPP propagation is at single interface, that is in between dielectric, having the positive dielectric constant ε_2 and metal, having the negative dielectric constant ε_1. For metal the bulk plasmon frequency will beω_p and the amplitude decays perpendicular to the $z-$ direction.

For the TM solutions in two spaces: dielectric and metal will be,
for z > 0,

$$\mathbf{H}_z(z) = A_2 e^{j\beta x} e^{-k_2 z}\,, \tag{3.27}$$

$$\mathbf{E}_x(z) = jA_2 \frac{1}{\omega \varepsilon_0 \varepsilon_2} k_2 e^{j\beta x} e^{-k_2 z}\,, \tag{3.28}$$

$$\mathbf{E}_z(z) = -A_1 \frac{\beta}{\omega \varepsilon_0 \varepsilon_2} e^{j\beta x} e^{-k_2 z}\,. \tag{3.29}$$

and for $z < 0$,

$$\mathbf{H}_y(z) = A_1 e^{j\beta x} e^{k_1 z}\,, \tag{3.30}$$

$$\mathbf{E}_x(z) = -jA_1 \frac{1}{\omega \varepsilon_0 \varepsilon_1} k_1 e^{j\beta x} e^{k_1 z}\,, \tag{3.31}$$

$$\mathbf{E}_x(z) = -A_1 \frac{\beta}{\omega \varepsilon_0 \varepsilon_1} e^{j\beta x} e^{-k_1 z}\,. \tag{3.32}$$

The continuity of $\mathbf{H}_y$ and $\varepsilon_i \mathbf{E}_z$ at the metal dielectric interface gives $A_1 = A_2$ and

$$\frac{k_2}{k_1} = -\frac{\varepsilon_2}{\varepsilon_1}\,. \tag{3.33}$$

The surface wave exists at the interface of metal dielectric with their real dielectric permittivity's opposite sign. We can therefore write,

$$k_1^2 \varepsilon = \beta^2 - k_0^2 \varepsilon_1, \tag{3.34}$$

$$k_2^2 \varepsilon = \beta^2 - k_0^2 \varepsilon_2\,. \tag{3.35}$$

The dispersion relation of SPPs propagation can be found as,

$$\beta = k_0\sqrt{\frac{\varepsilon_1\varepsilon_2}{\varepsilon_1+\varepsilon_2}}. \tag{3.36}$$

The TE surface modes can be expressed as,

$$\mathbf{E}_y(z) = A_2 e^{j\beta x} e^{-k_2 z}, \tag{3.37}$$

$$\mathbf{H}_x(z) = -jA_2\frac{\beta}{\omega\mu_0} k_2 e^{j\beta x} e^{-k_2 z}, \tag{3.38}$$

$$\mathbf{H}_z(z) = -A_2\frac{\beta}{\omega\mu_0} k_2 e^{j\beta x} e^{-k_2 z}. \tag{3.39}$$

and for z > 0,

$$\mathbf{E}_y(z) = A_1 e^{j\beta x} e^{-k_1 z}, \tag{3.40}$$

$$\mathbf{H}_x(z) = jA_1\frac{\beta}{\omega\varepsilon_0\varepsilon_1} k_1 e^{j\beta x} e^{k_1 z}, \tag{3.41}$$

$$\mathbf{H}_z(z) = A_1\frac{\beta}{\omega\varepsilon_0\varepsilon_1} k_2 e^{j\beta x} e^{k_1 z}. \tag{3.42}$$

$\mathbf{E}_y$ and $\mathbf{H}_x$ continuity requires for z < 0,

$$A_1(k_1 + k_2) = 0. \tag{3.43}$$

The surface needs that the real part of k_1 and k_2 should be more than zero for confinement. This will be satisfied if $A_1 = A_2 = 0$. Thus, no surface polarization modes for TE. SPP is only available for polarization in Transverse Magnetic mode[2].

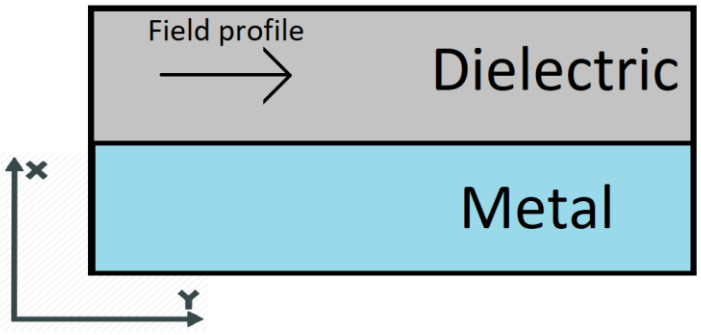

Fig. 3.2: SPP at the Single interface.

3.3 SPP at Double Interface

Two mostly used double interface configurations of SPP waveguides are: Dielectric-Metal-Dielectric (DMD), Metal-Dielectric-Metal (MDM). In these cases, SPPs are formed on both interfaces. When the distance is shorter than decay distance, it forms coupled mode of SPP. This coupled mode of propagation can also be sub-divided into even and odd modes, as shown in the Fig 3.3.

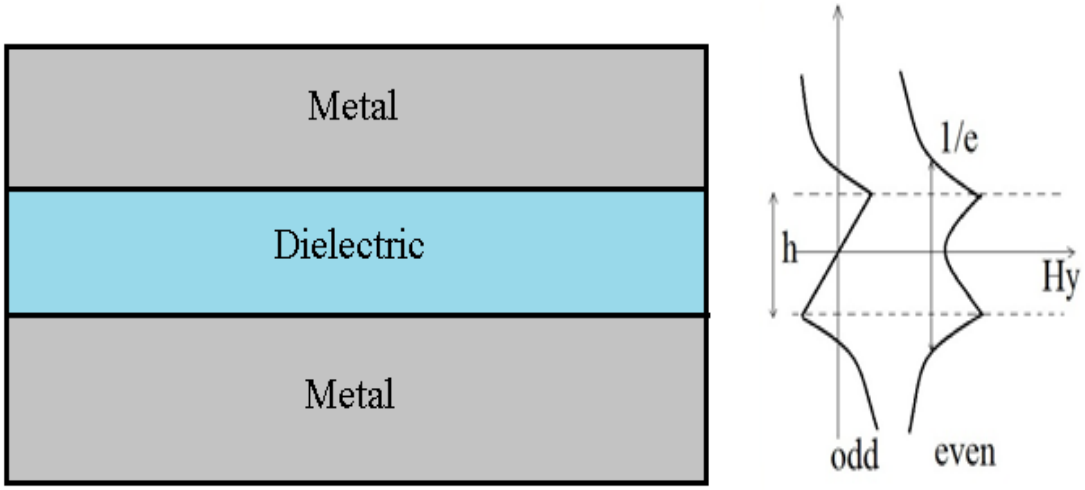

Fig. 3.3: SPP at the double interface.

Chapter 4

Overview of Numerical Analysis Methods

In order to design and analyze the proposed coupler, different approaches have been adopted. Initially FDTD (Finite Difference Time Domain) method was used in MATLAB. Later, the working tool was shifted to CST Studio Suite® where the calculations are done using FIT (Finite Integration Technique).

4.1 Finite Difference Time Domain (FDTD)

Finite-difference time-domain is a numerical analysis method used for modeling computational electrodynamics. The algorithm used in FDTD simulations is close to Yee algorithm. The original proposal was focused for homogeneous, isotropic and lossless media based on discretizing the volume into cells in Cartesian coordinates. The Yee algorithm intends to solve both the electric and magnetic fields based on the coupled Maxwell's curl equations instead of solving for either the electric field or the magnetic field alone with a wave equation.

The method starts with two of the Maxwell's equations,

$$\mathbf{D}\frac{\partial \mathbf{H}}{\partial t} = -\frac{1}{\mu}\nabla \times \mathbf{E}, \tag{4.1}$$

$$\mathbf{D}\frac{\partial \mathbf{E}}{\partial t} = \frac{1}{\varepsilon}\nabla \times \mathbf{H}. \tag{4.2}$$

The electric and magnetic fields are three dimensional vectors. Each equation can be converted into three coupled scalar first order differential equations. The derivatives are both in space and time. The curl operations of equations (4.1) and equation (4.2) yields the following six equations in Cartesian coordinates,

$$\frac{\partial \mathbf{E}_z}{\partial y} - \frac{\partial \mathbf{E}_y}{\partial z} = \mu\frac{\partial \mathbf{H}_x}{\partial t}, \tag{4.3}$$

$$\frac{\partial \mathbf{E}_x}{\partial z} - \frac{\partial \mathbf{E}_z}{\partial x} = \mu\frac{\partial \mathbf{H}_z}{\partial t}, \tag{4.4}$$

$$\frac{\partial \mathbf{E}_y}{\partial x} - \frac{\partial \mathbf{E}_x}{\partial y} = \mu \frac{\partial \mathbf{H}_z}{\partial t}, \tag{4.5}$$

$$\frac{\partial \mathbf{H}z}{\partial y} - \frac{\partial \mathbf{H}_y}{\partial z} = \varepsilon \frac{\partial \mathbf{E}_x}{\partial t}, \tag{4.6}$$

$$\frac{\partial \mathbf{H}x}{\partial z} - \frac{\partial \mathbf{H}_z}{\partial x} = \varepsilon \frac{\partial \mathbf{E}_y}{\partial t}, \tag{4.7}$$

$$\frac{\partial \mathbf{H}y}{\partial x} - \frac{\partial \mathbf{H}_x}{\partial y} = \varepsilon \frac{\partial \mathbf{E}_z}{\partial t}. \tag{4.8}$$

Then the scalar differential equations are transformed into difference equations. To achieve that, discretization is needed for both space and time. Yee visualized the field components being arranged within a unit cell for space discretization. Those unit cell edges store electric field components, while magnetic field components are stored in centers. The field components are arranged in such a way where **H** components are surrounded by four **E** components and vice versa, which leads to a spatially coupled system of field circulations corresponding to the law of Faraday and Ampere. The Fig 4.1 shows the Yee's spatial grid.

Considering a two-dimensional TM (Transverse Magnetic) polarized field case,

$$\frac{\partial \mathbf{E}_x}{\partial t} = \frac{1}{\varepsilon} \frac{\partial \mathbf{H}_z}{\partial y}, \tag{4.9}$$

$$\frac{\partial \mathbf{E}_y}{\partial t} = \frac{1}{\varepsilon} \frac{\partial \mathbf{H}_z}{\partial x}, \tag{4.10}$$

$$\frac{\partial \mathbf{H}_z}{\partial t} = \frac{1}{\mu} \left(\frac{\partial \mathbf{E}_x}{\partial y} - \frac{\partial \mathbf{E}_y}{\partial x} \right). \tag{4.11}$$

Central difference approximation is applied in each of the equations (4.9), (4.10) and (4.11) which finally conclude in a spatial scalar difference equations in (4.12), (4.13) and (4.14),

$$\frac{\partial \boldsymbol{E}_x}{\partial t} = \frac{1}{\varepsilon} \frac{\boldsymbol{H}_z(i,j) - \boldsymbol{H}_z(i,j-1)}{\Delta y}, \tag{4.12}$$

$$\frac{\partial \boldsymbol{E}_y}{\partial t} = \frac{1}{\varepsilon} \frac{\boldsymbol{H}_z(i,j) - \boldsymbol{H}_z(i-1,j)}{\Delta x}, \tag{4.13}$$

$$\frac{\partial \boldsymbol{H}_z}{\partial t} = \frac{1}{\mu}\left(\frac{\boldsymbol{E}_x(i,j+1)-\boldsymbol{E}_x(i,j)}{\Delta y} - \frac{\boldsymbol{E}_y(i+1,j)-\boldsymbol{E}_y(i-1,j)}{\Delta x}\right). \quad (4.14)$$

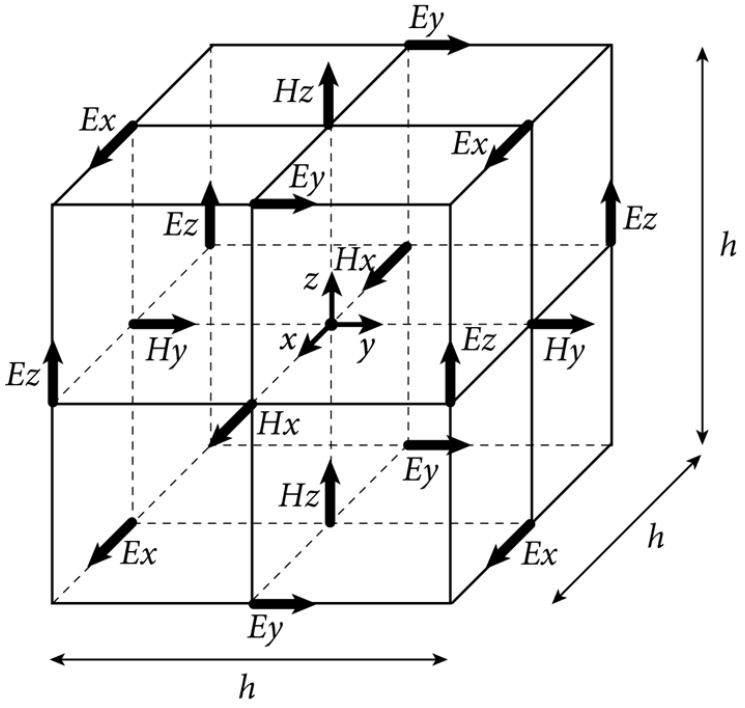

Fig. 4.1: Yee's spatial grid[17].

To consider the time derivatives, the time axis is to be considered as shown in the figures. The Electric and Magnetic field are mapped half a step apart along the time axis. Again, applying the central difference approximation the equations (4.12), (4.13) and (4.14) become,

$$\frac{\boldsymbol{E}_x^{n+1}\left(i+\frac{1}{2},j\right)-\boldsymbol{E}_x^{n}\left(i+\frac{1}{2},j\right)}{\Delta t} = \frac{1}{\varepsilon}\frac{\boldsymbol{H}_z^{n+\frac{1}{2}}\left(i+\frac{1}{2},j\right)-\boldsymbol{H}_z^{n+\frac{1}{2}}\left(i+\frac{1}{2},j-\frac{1}{2}\right)}{\Delta y}, \quad (4.15)$$

$$\frac{\boldsymbol{E}_y^{n+1}\left(i,j+\frac{1}{2}\right)-\boldsymbol{E}_y^{n}\left(i,j+\frac{1}{2}\right)}{\Delta t} = -\frac{1}{\varepsilon}\frac{\boldsymbol{H}_z^{n+\frac{1}{2}}\left(i+\frac{1}{2},j+\frac{1}{2}\right)-\boldsymbol{H}_z^{n+\frac{1}{2}}\left(i-\frac{1}{2},j+\frac{1}{2}\right)}{\Delta y}, \quad (4.16)$$

$$\frac{\boldsymbol{H}_z^{n+\frac{1}{2}}\left(i+\frac{1}{2},j+\frac{1}{2}\right)-\boldsymbol{H}_z^{n-\frac{1}{2}}\left(i+\frac{1}{2},j+\frac{1}{2}\right)}{\Delta t} = -\frac{1}{\mu}\left(\frac{\boldsymbol{E}_x^{n+1}\left(i+\frac{1}{2},j+1\right)-\boldsymbol{E}_x^{n}\left(i+\frac{1}{2},j\right)}{\Delta y} - \frac{\boldsymbol{E}_y^{n}\left(i+1,j+\frac{1}{2}\right)-\boldsymbol{E}_y^{n}\left(i,j+\frac{1}{2}\right)}{\Delta x}\right). \quad (4.17)$$

Simplifying the Yee's grid in 2D plane,

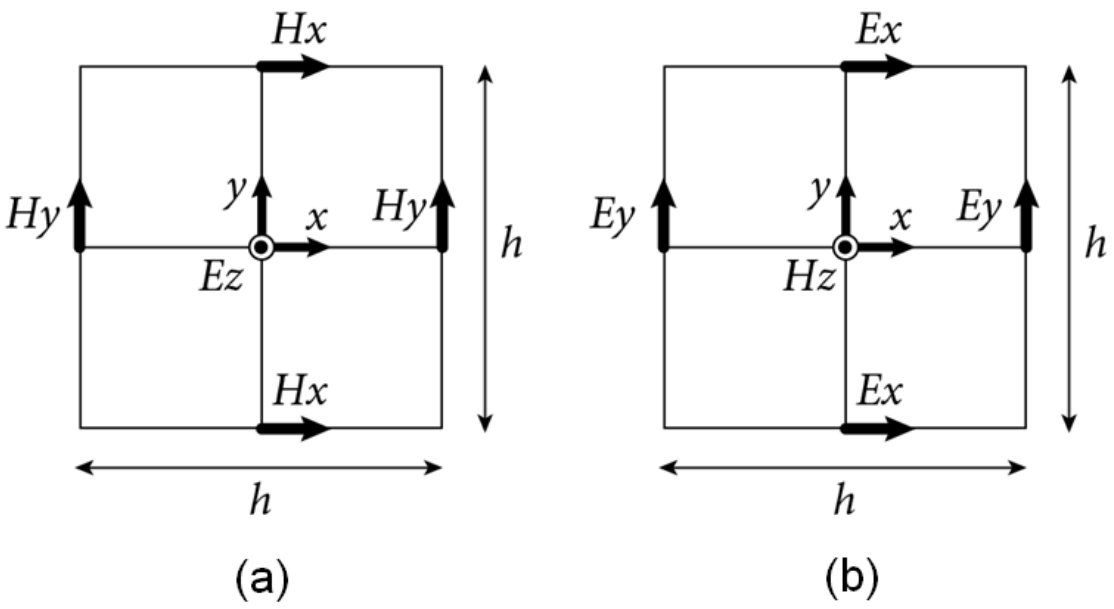

Fig. 4.2: Yee's grid in two dimensional plane[17].

Further simplification of Yee's grid for one dimension gives us,

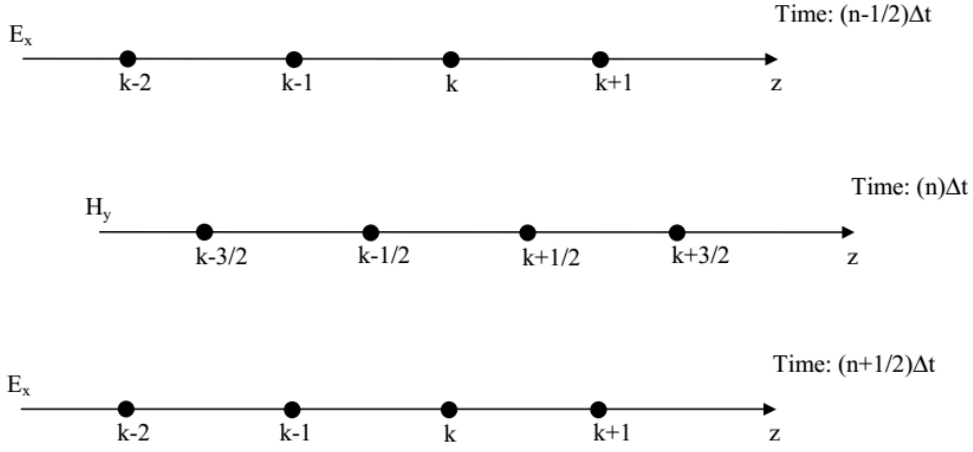

Fig. 4.3: Yee's grid in one dimension.

Each field component depends on the field of previous time step itself and the surrounding component in Yee's algorithm. For accurate results, the Yee grid must be

numerically stable. In an unstable algorithm the computed magnitude of electric and magnetic field components will gradually increases, making the system unstable. The EM field's propagation should not be faster than the allowed limit imposed by the phase velocity within the material to insure numerical stability. This is done by limiting time step Δt using the Courant-Friedrich-Lewy criterion for the general Yee FDTD grid as follows,

$$\Delta t \leq \left\{ \frac{1}{v_p \sqrt{\frac{1}{(\Delta x)^2}+\frac{1}{(\Delta y)^2}+\frac{1}{(\Delta z)^2}}} \right\}, \tag{4.18}$$

where, Δx, Δy and Δz indicates the spatial Cartesian grid increments.

4.2 Perfectly Matched Layer (PML)

In the FDTD model, a space that is infinitely extending theoretically is converted into a finite computational cell as there are limitations on computer resources. It is said that the boundary is preferably absorbent without any nonphysical reflection back to the concerned area. A number of boundary conditions have been proposed to implement this , namely the perfectly matched layer of Berenger[18].

It is an engineered absorbing layer for wave equations which is commonly used in numerical methods to append computational regions to simulate open boundary problems.

The main feature that distinguishes PML from an ordinary absorbing material is that waves incident on PML from non-PML medium do not reflect at the interface. This property allows PML to strongly absorb outgoing waves from interior of a computational region without reflecting back into the interior.

4.3 Finite Integration Technique (FIT)

Initial works were based on FDTD (Finite Difference Time Domain). AS we progressed working with FDTD was getting a bit complex. So, working tool was shifted from MATLAB to CST, and CST is a three-dimensional Electromagnetic analysis software which works on the basis of FIT (Finite Integration Technique).

FIT is a numerical technique to solve different electromagnetic wave equations. It was first introduced by T. Weiland in 1977[17]. Discretization method of FIT is similar to the one of FDTD method for homogenous media. Only difference is that, FIT works with the integral form of Maxwell's equations. A set of staggered grids are made from the equations and the calculations are then performed on them. The most common drawback of FIT is the usage of Yee's Cartesian meshes, they become inflexible when non orthogonal and complex structures are taken into consideration.

Here, one dimensional grid is first made then three one dimensional grids available for three different axes are combined together for further calculations. Maxwell's equations can be discretized in this way into a three-dimensional staggered grid in Cartesian coordinate. Let, a staggered grid on one –dimension having interval is [0, L], where 0 = $x_0 < x_1, \ldots\ldots, x_m$ = L is a finite sequence of n grid points.

This one –dimensional grid can also be described as- $x_i = i * \frac{L}{n}, i = 0, \ldots.$, n. Here, the grid has mesh size, h= $\frac{L}{n}$ .And the corresponding staggered grid can be described in similar fashion- $s_i = (i - 0.5) * \frac{L}{n}, i$ =1,…, n. Like the grid shown in Fig 4.4.

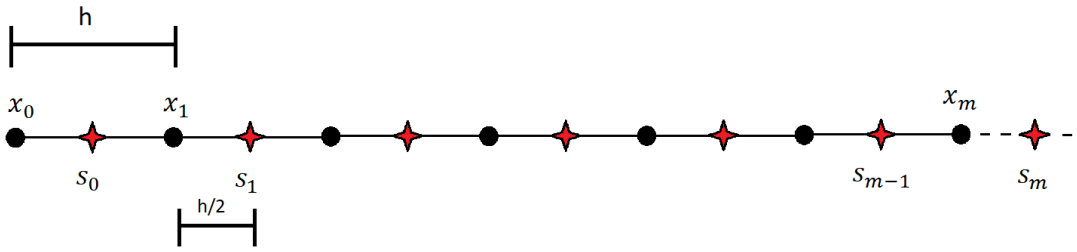

Fig. 4.4: Uniform grid x_i and s_i corresponding staggered grid in one dimension.

Now, a set of corner points can be defined as,

$$\Omega_c := \{x_0, x_1, \ldots\ldots, x_m\}. \tag{4.19}$$

And corresponding staggered grid points can be defined as,

$$s_i := \frac{1}{2}(x_i + x_{i+1}) \quad \text{for i= 0,…..m-1.} \tag{4.20}$$

Which indicates an increment in space of $\frac{h}{2}$ .Eventually forming a staggered grid corresponding Ω_c ,

$$\Omega_s := \{s_0, s_1, \dots \dots, s_{m-1}\}. \tag{4.21}$$

For defining a staggered grid in three-dimension, rectangular domain is considered,

$$\Omega = [0, L_x] \times [0, L_y] \times [0, L_z]. \tag{4.22}$$

Furthermore, it is assumed that $[0, L_x], [0, L_y], [0, L_z]$ one-dimensional intervals are discretized by one-dimensional grids,

$$\Omega_c^x = \{ x_0, x_1, \dots ., x_m\}, \tag{4.23}$$

$$\Omega_c^y = \{ y_0, y_1, \dots ., y_m\}, \tag{4.24}$$

$$\Omega_c^z = \{ z_0, z_1, \dots ., z_m\}. \tag{4.24}$$

Which are set of grid points in x,y and z direction. This leads to 8 possible types of grids in Ω ,such as,

$$\Omega_{t_x,t_y,t_z} = \Omega_{t_x}^x \times \Omega_{t_y}^y \times \Omega_{t_z}^z. \tag{4.25}$$

Where = $(t_x, t_y, t_z) = \{c, s\}^3$ and c denotes corner points and s denotes staggered points. Using these grids all the calculations in FIT are done[19].

4.4 CST

Analysis and design of the couplers were done in CST Studio Suite ®. It is an extremely user-friendly software, largely used to model, test and customize devices and structures for electromagnetic (EM) applications; such as- analysis of antennas, filters, couplers, planar and multi-layer structures and SI and EMC effects. It offers the flexibility to use Time Domain solver and the Frequency Domain solver, beside the flagship module. The analysis technique used here is FIT (Finite Integration Technique)[20].

Chapter 5

Designing of Efficient Nano-plasmonic Couplers

Coupling is the process which allows the transfer of energy from one medium (i.e. optical fiber, metallic wire) to another. Transferring electrical energy from one portion of the circuit to the next portion is also known as coupling. Coupling between two waveguides in nano scale in plasmonic circuits is known as nano-plasmonic coupling.

Surface plasmons (SP) are electromagnetic waves that propagate along the planar interface between a metal and dielectric medium due to the coherent oscillations of delocalized electrons. SPs occur at the interface between a metal and a dielectric material. These waves are locked close to the surface due to the interaction with the electrons which are located at the surface of a metallic material. The resonant interplay between the EM field of light and electron-charged vibrations near the metal surface gives rise to SP and also contributes to the unique characteristics. As generation of SPs require abundance of free electrons, plasmonic waveguides are made of metals[21].

The penetration of SPs into metal is approximated by skin depth. It can be roughly 10 nm- which is less than the wavelength of light in free space by two orders of magnitude. This characteristic of SPs creates the possibility to localize light in metallic structures which are of subwavelength dimensions. It can play a pivotal role in the construction of scaled down optoelectronic circuits and overcome the size limitation problem of photonic circuits. Furthermore, Interbrand transition of electrons causes loss of energy in metals at the optical range. Even the best of conductors is blighted by these losses. It causes degradation of performance of plasmonic devices. Metal-dielectric-metal composition of plasmonic waveguide can achieve high confinement. But it increases propagation loss due to the larger area available for the field to overlap with the metallic layers. In order to minimize the propagation loss, the dielectric waveguide as well as the plasmonic waveguide are integrated on a single chip. The dielectric waveguide receives optical signal from the source and couples the signal to the metal-dielectric-metal (MDM) waveguide. This initiates the necessity of

effective coupling of optical signals from dielectric waveguide to plasmonic waveguide. Therefore, it is imperative to design efficient nano-plasmonic coupling structures with different materials for the miniaturization of photonic devices[22].

5.1 Choice of Materials

The most prominent losses in plasmonic waveguides occur due to inter band transition. The valence band electrons of dielectric materials ingest energy from incident photons and jump from valence band to conduction band. This in turn creates inter band transition losses[23]. To lessen these losses materials with greater bandgap are preferred. In our nano-plasmonic couplers GaAs is chosen as dielectric waveguide. GaAs is a type III / V semiconductor with high electron mobility and a high condensed electron velocity relative to silicon. The bandgap of GaAs is1.441eV which is ideal for minimizing inter band transition losses. Furthermore, GaAs based modules are not thermally sensitive due to their large band gap. Silver is chosen as metal in MDM (Metal Dielectric Metal) waveguide due to its dispersive properties. Some of the favorable Dielectrics that could be chosen based on their bandgap are given below- GaAs, Cu_2O[22], SiO_2, AlAs, Al_2O_3, GLS, Si[24].

5.2 Analysis Methodology

Finite integration technique (FIT) has been deployed to explore the output characteristics of the hypothetical coupler. This method was proposed by Thomas Weiland[25]. FIT discretizes the integral form of Maxwell's equations and converts those equations to a set of grids. Thus, making them appropriate for computer simulation. EM field problems can be solved numerically in time and frequency domain using FIT. CST MICROWAVE STUDIO® (CST MWS), a 3D electromagnetic (EM) simulation software, has been employed as the simulation tool. This software can solve EM field problems in both frequency and time domain. Time domain solver was used in our simulations. Perfectly matched layer (PML) was applied at every boundary of simulation domain. Hexahedral mesh property has been implemented in the simulation settings.

Input port has been placed on dielectric waveguide and output port has been placed on the MDM waveguide. To determine the performance specifications, fundamental mode has been

excited at the input port and power was measured both on input and output port. Coupling efficiency is defined as the ratio of the power incident at MDM waveguide and the power incident on the dielectric waveguide. To avoid radiative effect while computing power, the output port was taken 10 nm away from the waveguide junction[26].

5.3 Designing Structures

5.3.1 Rectangular Structure

A three-dimensional dielectric rectangular waveguide coupled with a plasmonic waveguide of MDM (metal-dielectric-metal) was selected. Fig. 5.1 displays the schematic of the proposed plasmonic coupler. The width of the dielectric material (Gallium Arsenide) has been kept 500 nm. The height considered as parameter ‘c’ is kept 300 nm.

The air gap presents between GaAs and MDM waveguide, defined as ‘b’ is kept 10 nm initially. As the choice of material, silver as metal and air as dielectric were chosen. The total width of the MDM waveguide is 340 nm having air medium between silver, whose width is specified as ‘a’ and the value is chosen to be 90 nm. To find the appropriate value of ‘a’ for which the coupling efficiency is optimum, computational simulations have been deployed. In similar fashion ‘b’ and ‘c’ are also found.

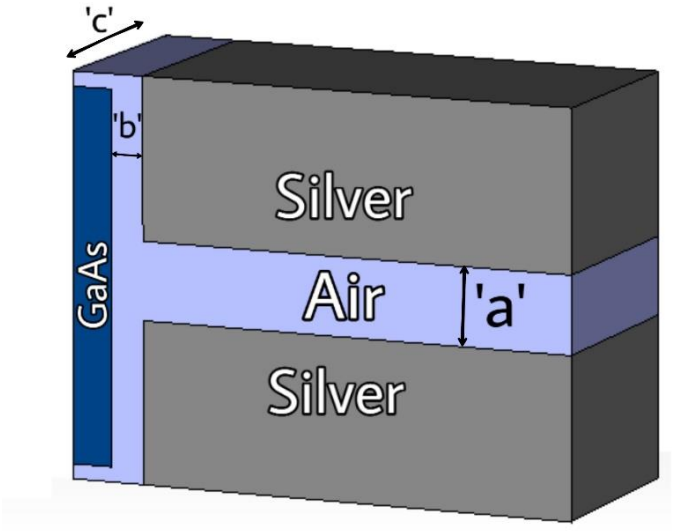

Fig. 5.1: Three-dimensional view of proposed air gap based rectangular GaAs nano-plasmonic coupler.

5.3.2 Semi-Elliptical Structure

Here the width of the plasmonic waveguide is defined by the parameter 'ω_a'. The height of the structure is defined by the parameter 'h'. As we are dealing with a semi elliptical structure, two other parameters are considered which are semi major axis and semi minor axis. We can express an ellipse using the following equation,

$$\frac{x^2}{p^2} + \frac{y^2}{q^2} = 1, \tag{5.1}$$

here, p = semi-minor axis,

q = semi-major axis and q > p.

The width of the dielectric waveguide is defined by$\omega_g$where, ω_g = 2q.

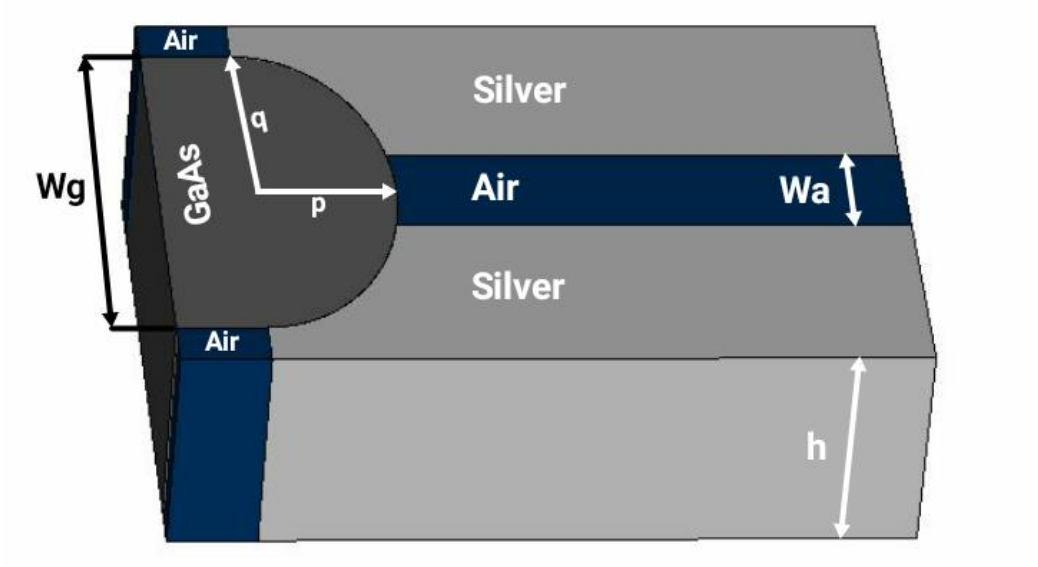

Fig. 5.2: Three-dimensional view of proposed Semi elliptical coupling structure.

In the simulations, the width of the dielectric waveguide, width of the plasmonic waveguide, semi-minor axis and the height of the coupling structure have been subsequently varied. Simulations were carried out at wavelengths ranging from 1000 nm to 2000 nm.

5.4 Optimization of structures

5.4.1 Rectangular Structure

After the design of the coupler has been completed, main focus was given to performance parameters. Initially performance parameters for initial structure was checked by putting two ports at two certain places of the coupler. Port-1 was placed at the left most side, at the upper portion of GaAs layer, a Gaussian pulse was sent via port-1 and another port, port-2 was placed 35 nm away from the GaAs layer. Port-2 received the transferred signal through the proposed coupler. CST prepared all the performance parameters for different wavelengths using FIT (Finite Integration Technique).

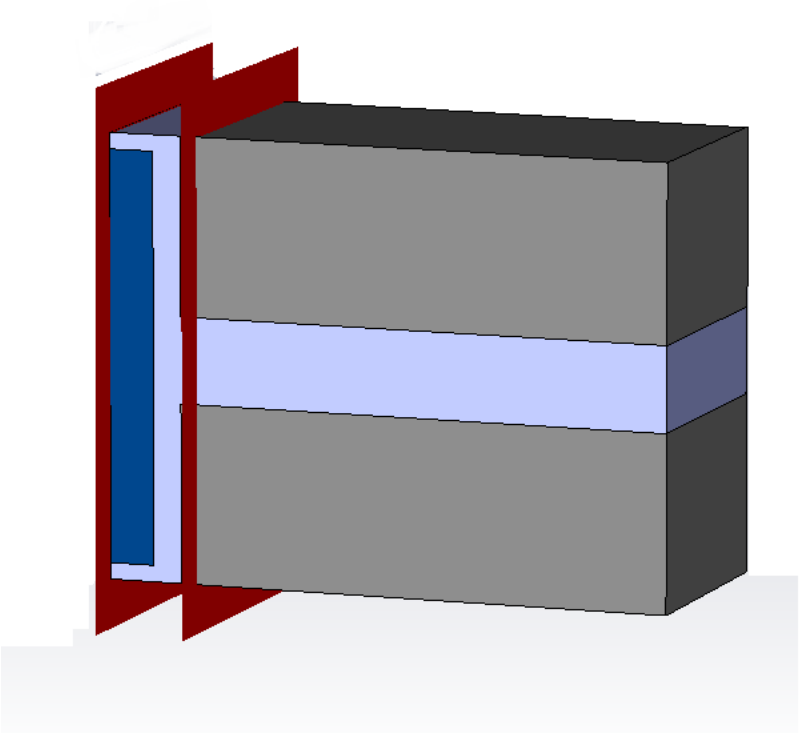

Fig. 5.3: Proposed rectangular coupler with the ports.

In order to find the optimum dimension of our chosen parameters, ‘a’, ‘b’ and ‘c’ are varied keeping the width of the GaAs unchanged at w = 500 nm. Primarily, considering ‘b’= 10 nm and ‘c’= 300 nm, the transmittance efficiency for the proposed coupler was calculated varying ‘a’ in the range 40 nm < a<130 nm. The results have been demonstrated in the Fig. 5.4 and Fig 5.5.

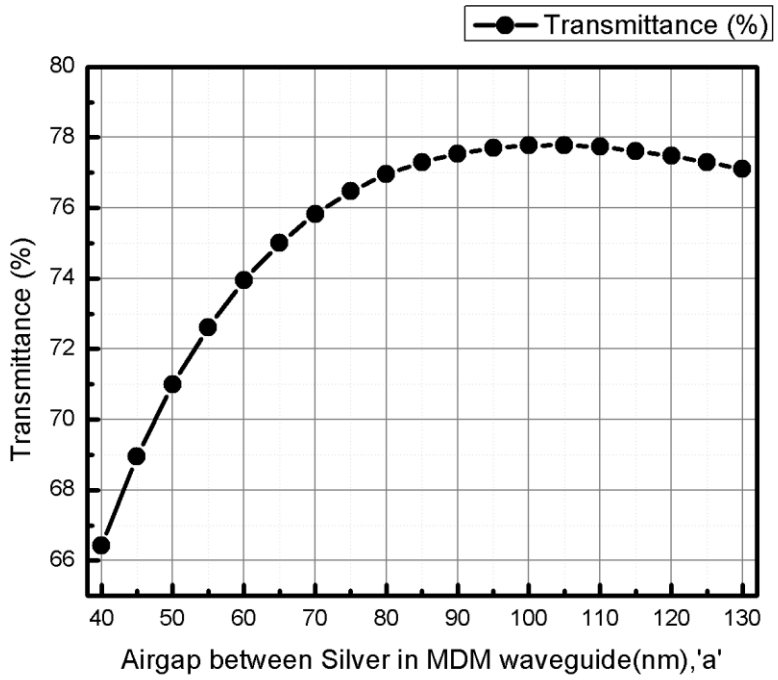

Fig. 5.4: Transmittance vs variation of ‘a’, when ‘b’=10 nm and ‘c’=300 nm.

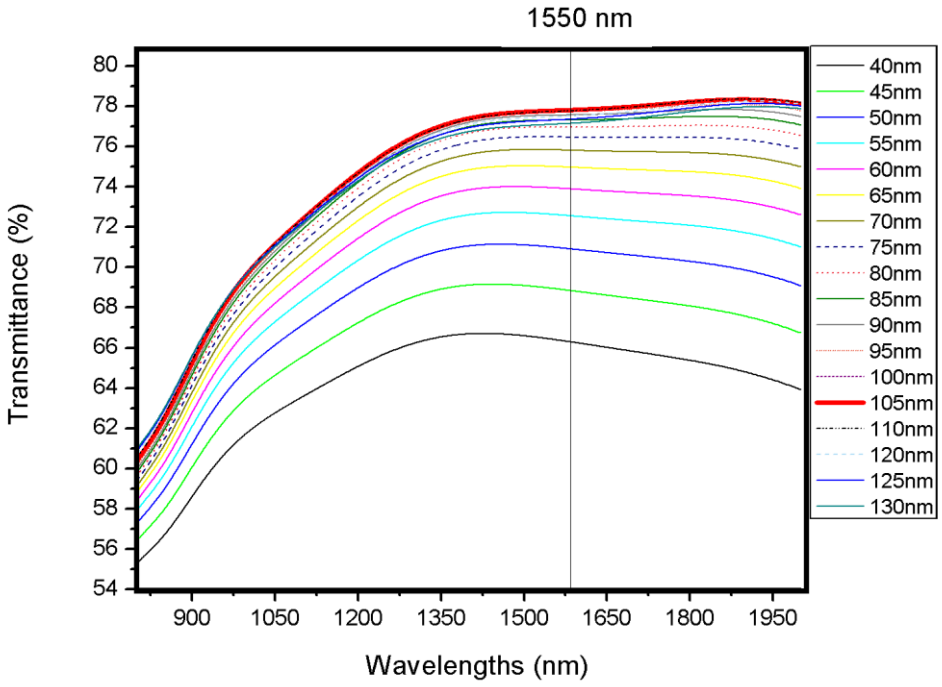

Fig. 5.5: Transmittance vs wavelengths for variation of ‘a’.

It can be observed that the transmittance is comparatively low at ‘a’= 40 nm and the measured value increases with the increment of ‘a’. After sufficient amounts of simulations, optimum transmittance (at communication wavelength of 1550 nm) was found at ‘a’= 105 nm.

Next, keeping the value of ‘a’ fixed at 105 nm, ‘b’ was varied in the range 0 nm <b < 20 nm. The transmittance of the coupler was recorded in similar fashion like the previous case and the optimum value of ‘b’ for better transmission was found to be 11 nm. The results can be observed in Fig. 5.6 and Fig. 5.7.

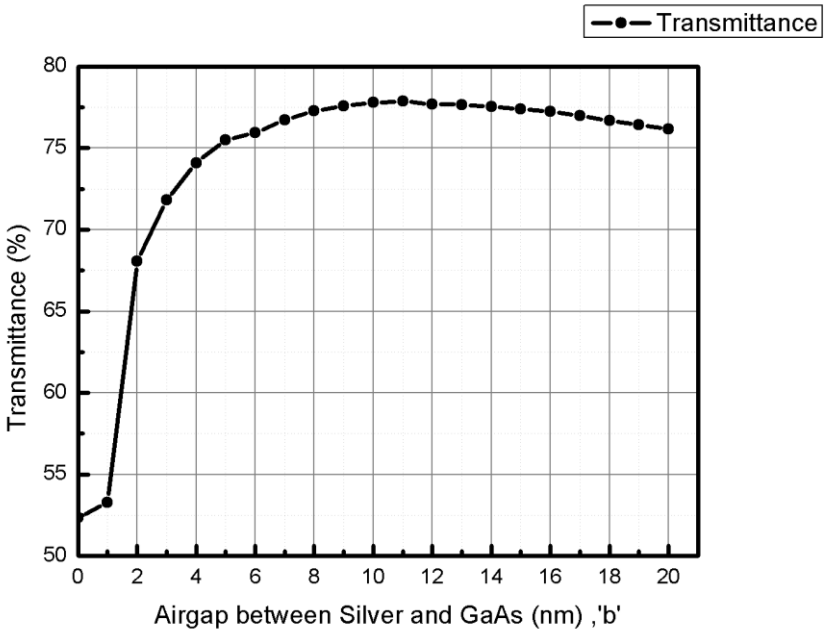

Fig.5.6: Transmittance vs variation of ‘b’, when ‘a’=105 nm and ‘c’ = 300 nm.

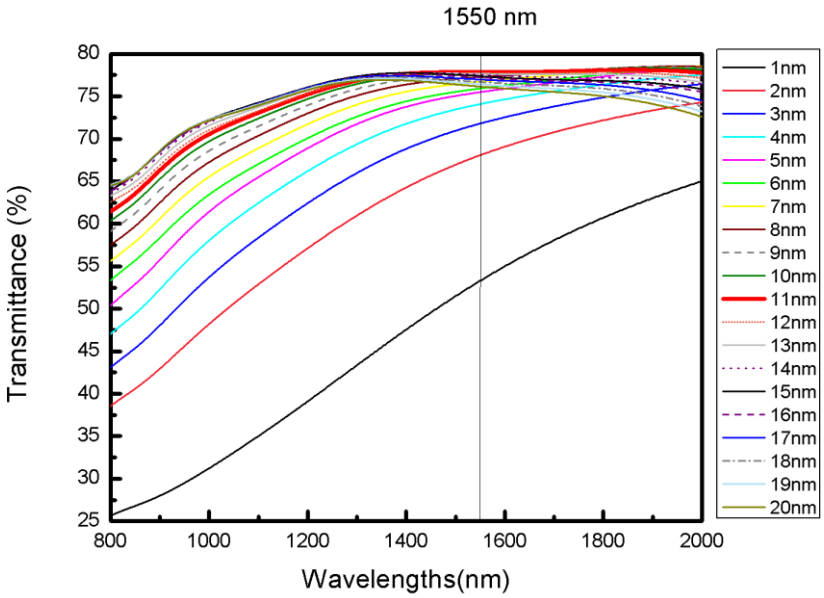

Fig. 5.7: Transmittance vs wavelengths for variation of 'b'.

Once the optimum dimensions of 'a' and 'has been found, the value of 'c' has been varied next, from 50 nm ascending to 500 nm. In this case, the best value for transmittance has been calculated at 'c'= 300 nm represented by Fig. 5.8 and Fig. 5.9.

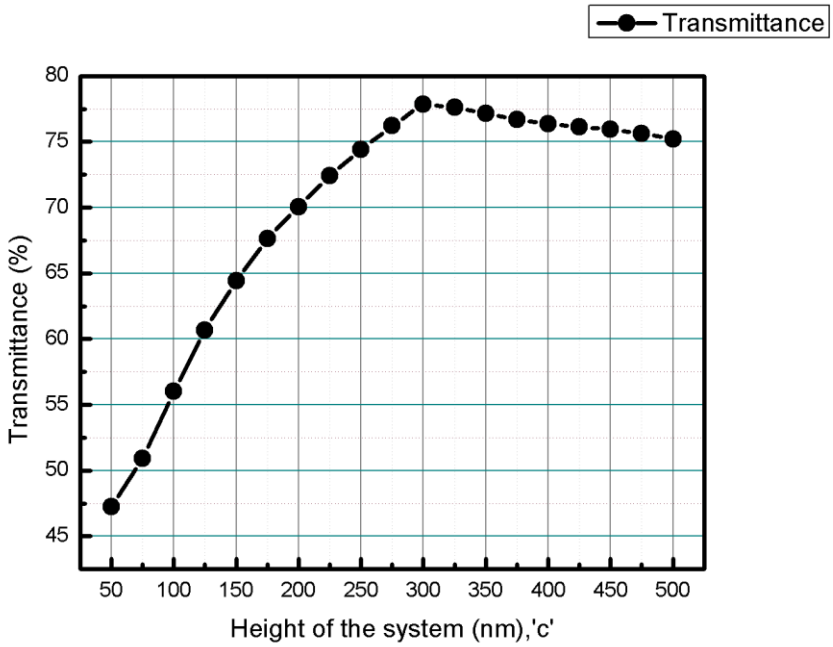

Fig. 5.8: Transmittance vs variation of 'c', when 'a'=105 nm and 'b'=11 nm.

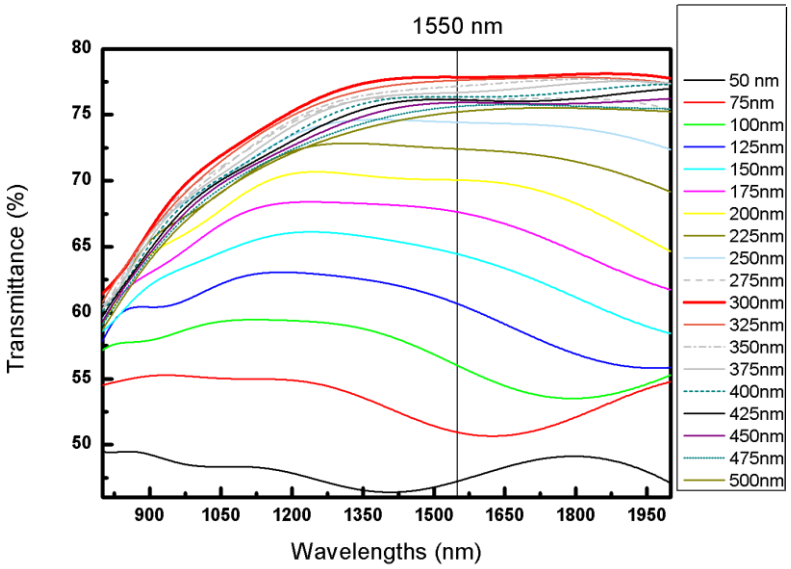

Fig. 5.9: Transmittance vs wavelengths for variation of 'c'.

The optimum dimensions were therefore finalized as air gap between silver, 'a'= 105 nm, air gap between GaAs and silver, 'b'= 11 nm and the height of the coupler, 'c'= 300 nm.

5.4.2 Semi-Elliptical Structure

Port-1 was placed at the left most side of the proposed structure. Port two was placed 95 nm away from port-1. A Gaussian pulse was sent via port-1. Port-2 received the transmitted signal through the dielectric coupler. CST calculated all the performance parameters for different wavelengths applying finite integration technique (FIT).

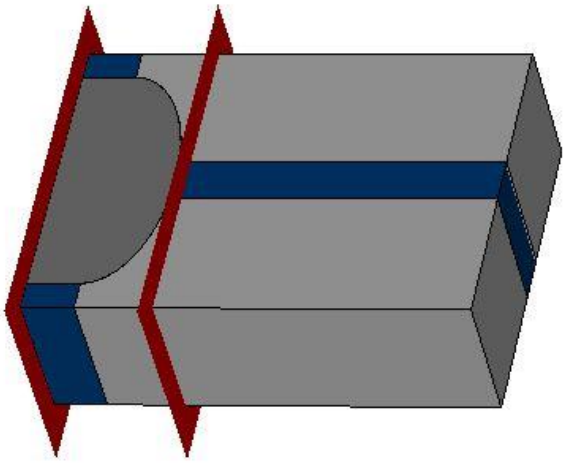

Fig. 5.10: Proposed semi-elliptical coupler with ports.

Taking the height of the structure has 300 nm and the width of the plasmonic waveguide as 40 nm, we have varied the width of the dielectric waveguide, 'ω_g', from 280nm to 420 nm. During this process the length of semi-minor axis was kept fixed at 50 nm. The coupling efficiencies at the optical communication wavelength of 1550 nm, found at the aforementioned dimensions are shown in Fig 5.11. Coupling efficiencies, at the wavelengths ranging from 1000 nm to 2000 nm due to the variation of 'ω_g', has been depicted in Fig 5.12.

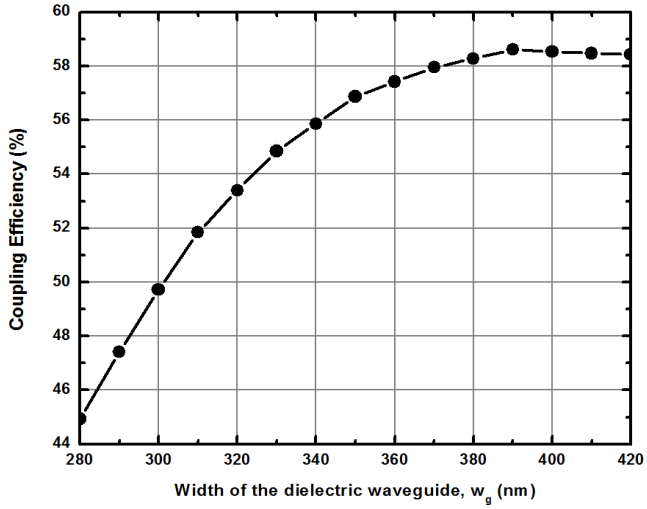

Fig. 5.11: Coupling Efficiency vs width of dielectric waveguide, 'ω_g'.

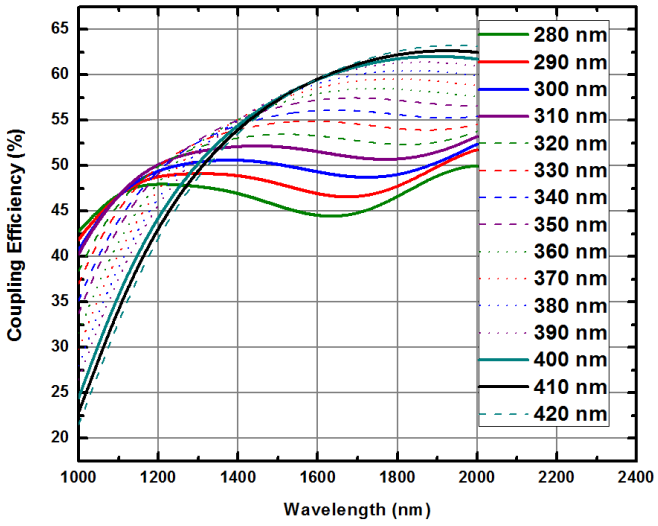

Fig. 5.12: Coupling Efficiency vs Wavelength for different 'ω_g'.

From Fig 5.10 it is evident that 'ω_g' = 390 nm yields the highest coupling efficiency. We have continued further optimization of the structure by taking 'ω_g' as 390 nm. Keeping 'ω_g' at 390 nm, we have varied the width of the plasmonic waveguide from 20 nm to 100 nm. The resulting coupling efficiencies (at 1550 nm) due to this variation have been presented in Fig 5.13. From this figure we can observe that at 'ω_a' = 70 nm, coupling efficiency reaches the highest value. Coupling efficiencies at the above-mentioned wavelength range due to the change of 'ω_a' has been shown in Fig 5.14.

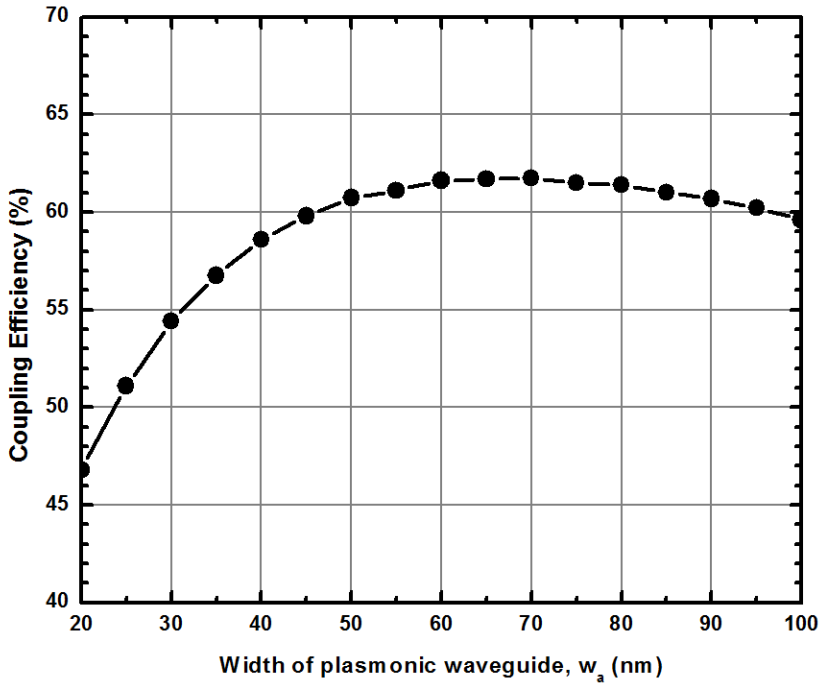

Fig. 5.13: Coupling Efficiency vs width of plasmonic waveguide 'ω_a' (here, 'ω_g' = 390 nm).

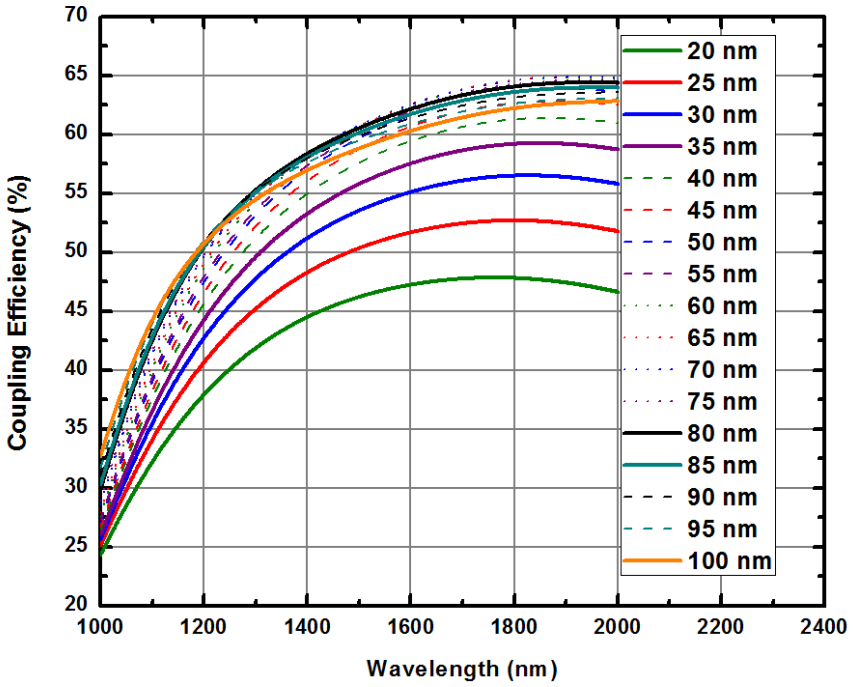

Fig. 5.14: Coupling Efficiency vs Wavelength for different 'ω_a'.

Afterwards we have varied the length of semi-minor axis from 30 nm to 120 nm keeping 'ω_g' = 390 nm and 'ω_a' = 70 nm. The variation of coupling efficiencies (at 1550 nm) due the variation of the semi-minor axis has been plotted in Fig 5.15. From this graph, it is observed that coupling efficiency (1550 nm) doesn't vary much due to the variation of 'p'. In Fig 5.16, the coupling efficiencies at the same wavelength range due to the modification of 'p' have been demonstrated.

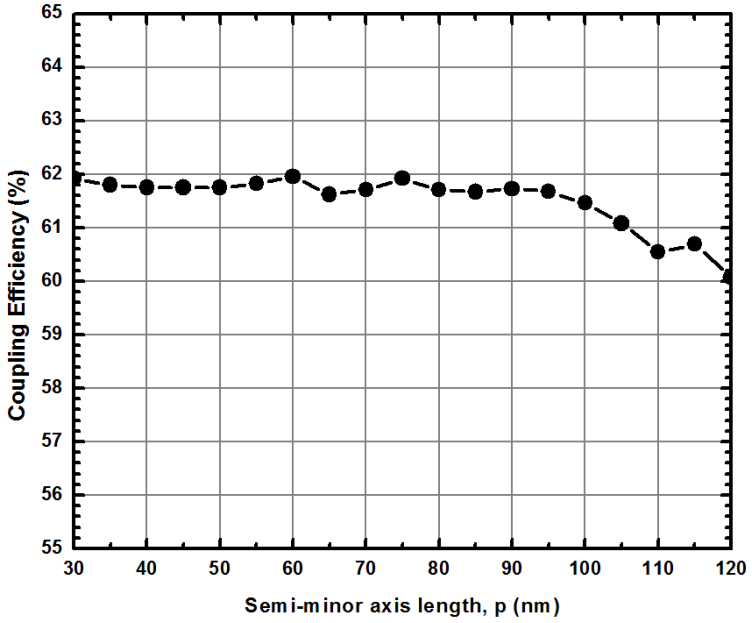

Fig. 5.15: Coupling Efficiency vs semi-minor axis length, 'p' (here, 'ω_g' = 390 nm, 'ω_a' = 70 nm).

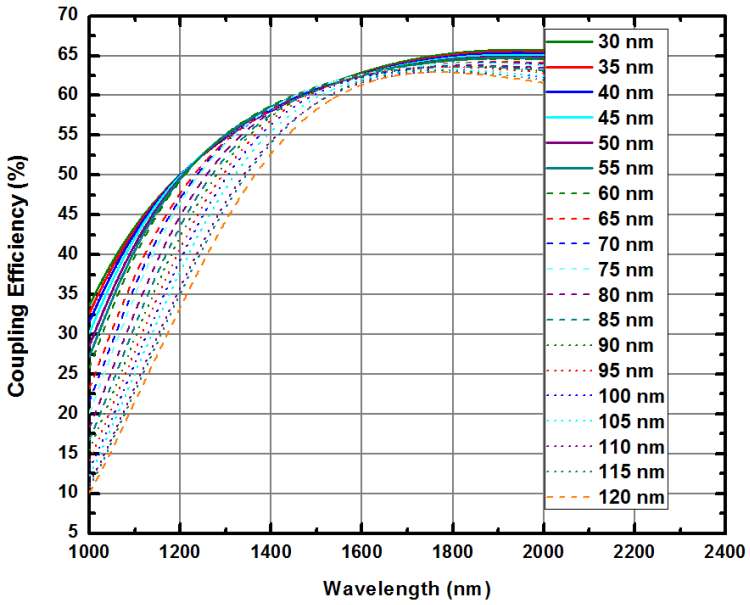

Fig. 5.16: Coupling Efficiency vs Wavelength for different 'p'.

Finally, taking ‘p’ = 60 nm, we have varied the height of the structure, ‘h’, from 140 nm to 300 nm. From Fig 5.17 we can observe that the coupling efficiency (at 1550 nm) reaches its peak (63.169%) at ‘h’ = 210 nm. In Fig. 5.18, we can observe the coupling efficiencies from 1000 nm to 2000 nm wavelength range because of the variation of ‘h’.

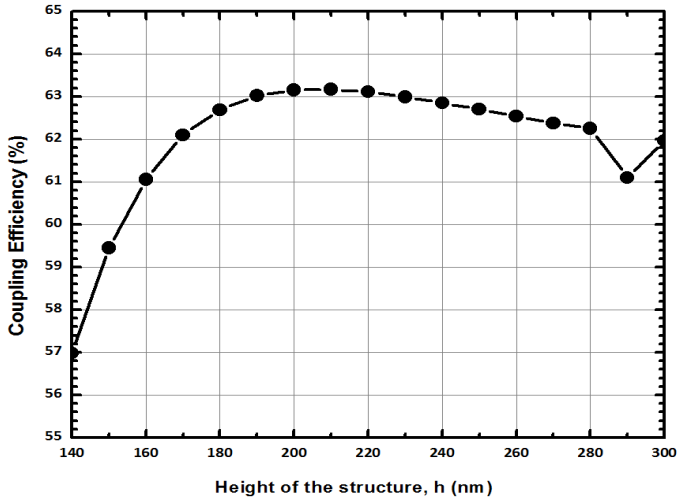

Fig. 5.17: Coupling Efficiency vs height of the structure, ‘h’ (here, ‘ω_g’ = 390 nm, ‘ω_a’ = 70 nm, ‘p’ = 60 nm).

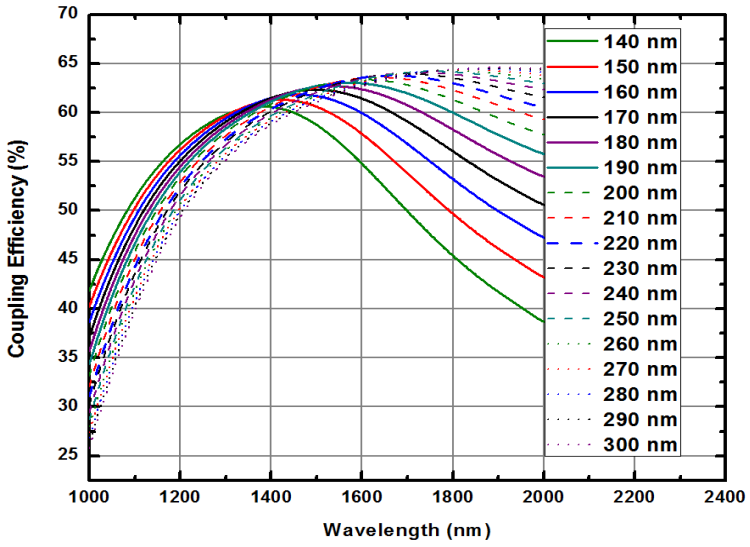

Fig. 5.18: Coupling Efficiency vs Wavelength for different ‘h’.

5.5 Performance characteristics of the optimized structures

5.5.1 Rectangular Structure

The proposed coupler yields coupling efficiency of 77.83% when ‘a’= 105 nm, ‘b’= 11 nm and ‘c’= 300 nm. This optimum coupling efficiency has been achieved after quite a few numbers of simulations. All the performance parameters have been measured at such configuration. Transmittance, absorbance and reflectance have been detected at different wavelengths and the results are in Fig. 5.19, Fig 5.20, Fig 5.21. Different performance specifications at the optical communication wavelength (1550 nm) have been inspected and are tabulated in Table 5.1. The values of transmitted power, reflected power and absorbed power are calculated and presented in Table 5.1, whose sum is found to be equal to 1, which is expected.

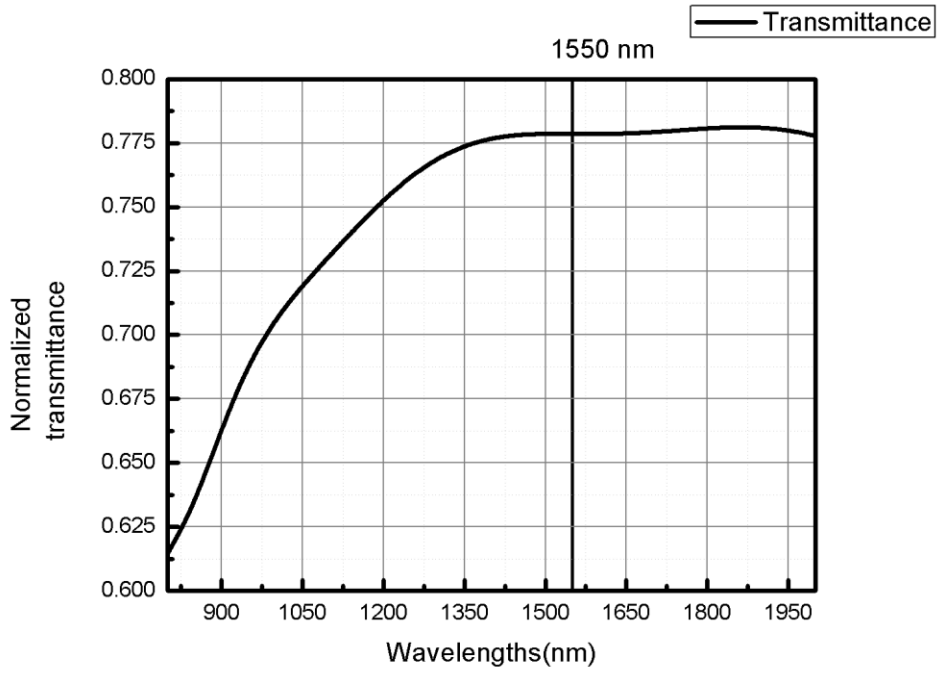

Fig. 5.19: Transmittance vs Wavelength.

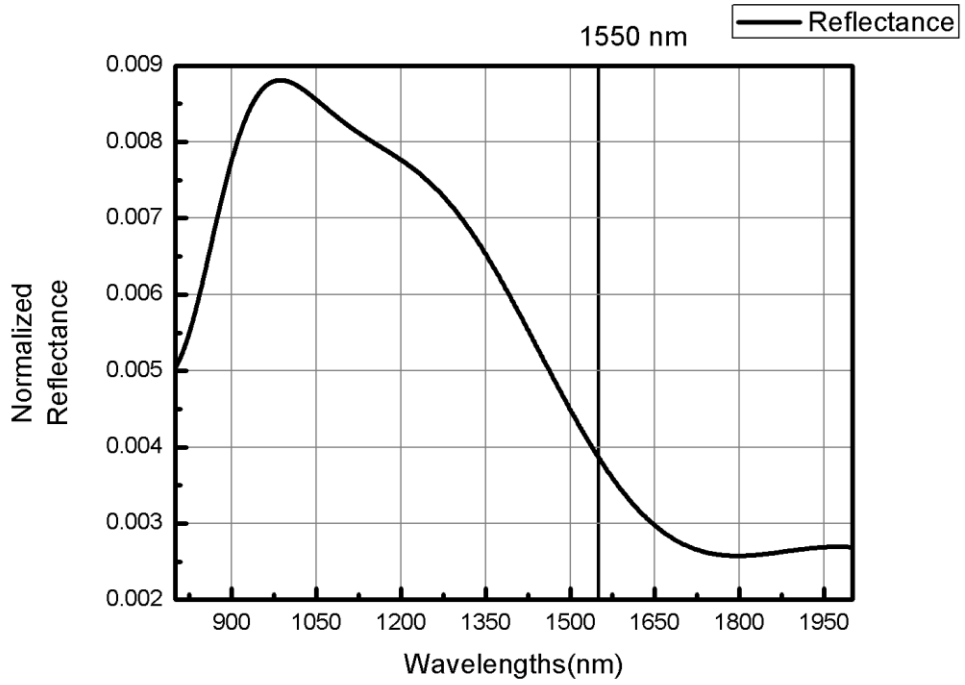

Fig. 5.20: Reflectance vs Wavelength.

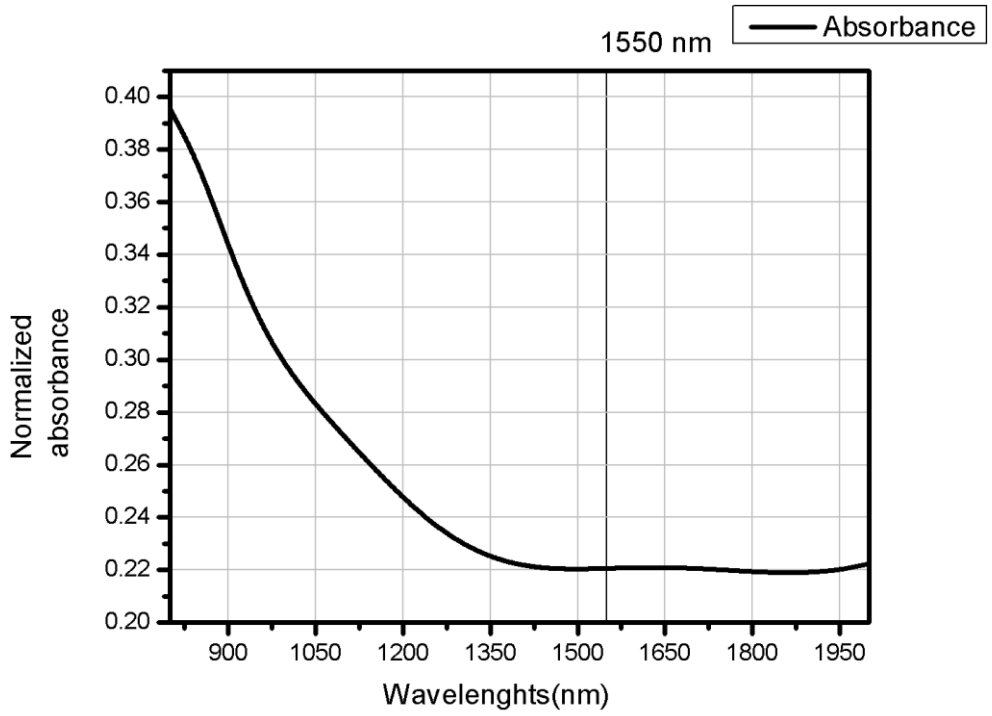

Fig. 5.21: Absorbance vs Wavelength.

Electrical field distribution of the coupler is observed at optical communication wavelength (1550 nm) which is shown in Fig. 5.22 and Fig 5.23. The color map suggests that the field strength is much lower in the metal region than in the dielectric region. Higher loss component in metal contributes to the aforesaid phenomenon.

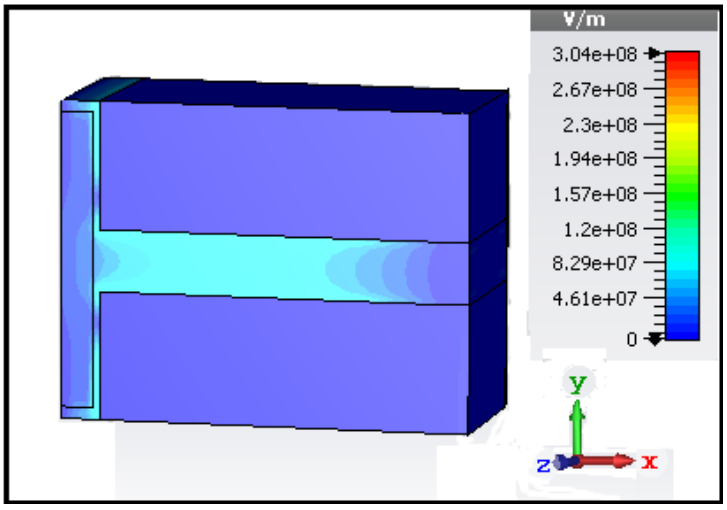

Fig. 5.22: Electric field distribution(3D).

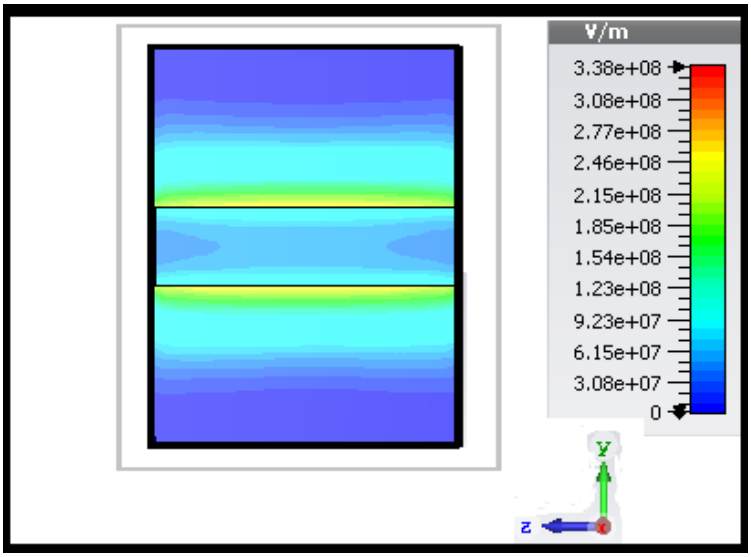

Fig. 5.23: Electrical field distribution (Cross sectional view of the coupler)
Cross section taken 40 nm away from GaAs Layer.

Table 5.1: Values of different performance parameters at optical communication wavelength (1550 nm)

Sl. No.	Parameters	Values
1	Transmittance	0.77839
2	Reflectance	0.00362
3	Absorbance	0.21799

5.5.2 Semi-Elliptical structure

The proposed coupler yields coupling efficiency of 63% when 'ω_g' = 390 nm, 'ω_a' = 70 nm, 'p' = 60 nm and 'h' = 210 nm. Using the optimum dimensions for the proposed plasmonic coupler, simulations have been carried out to obtain various performance parameters such as coupling efficiency, reflectance and absorbance for a wavelength range of 1000nm to 2000 nm and depicted in Fig 5.23, Fig 5.24 & Fig 5.25.

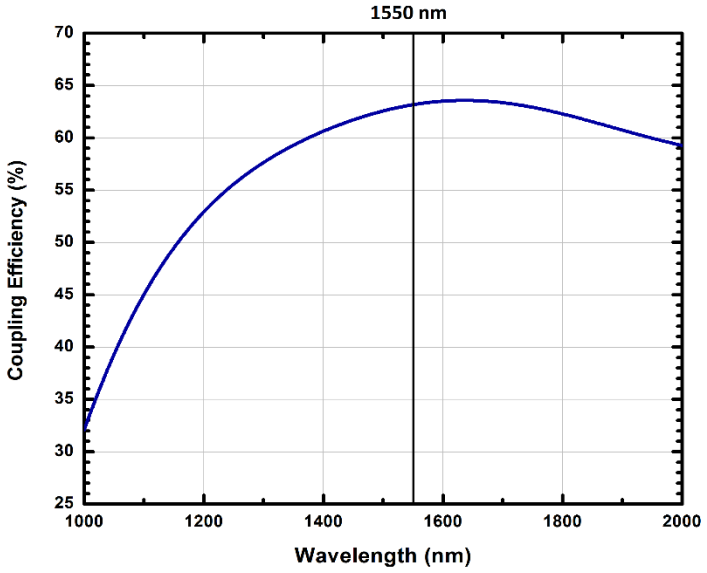

Fig. 5.24: Coupling Efficiency vs Wavelength.

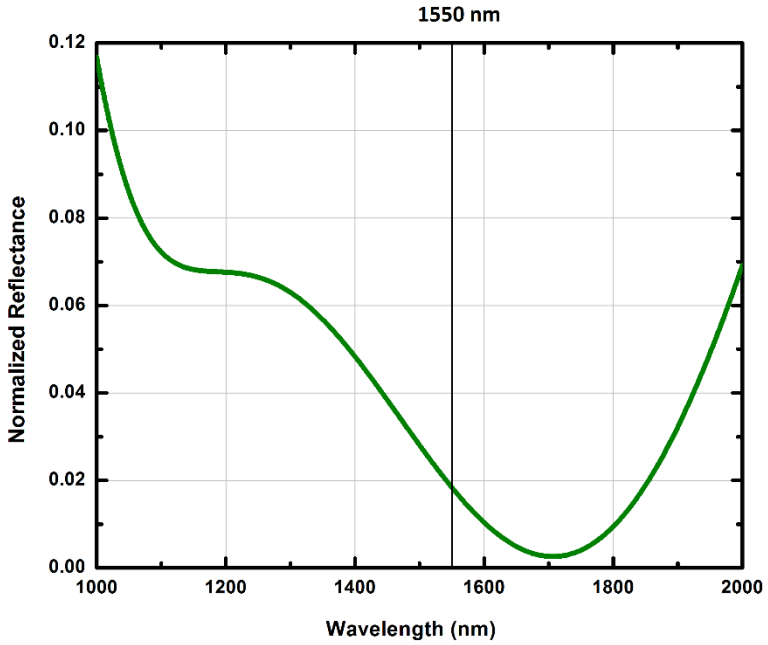

Fig. 5.25: Normalized Reflectance vs Wavelength.

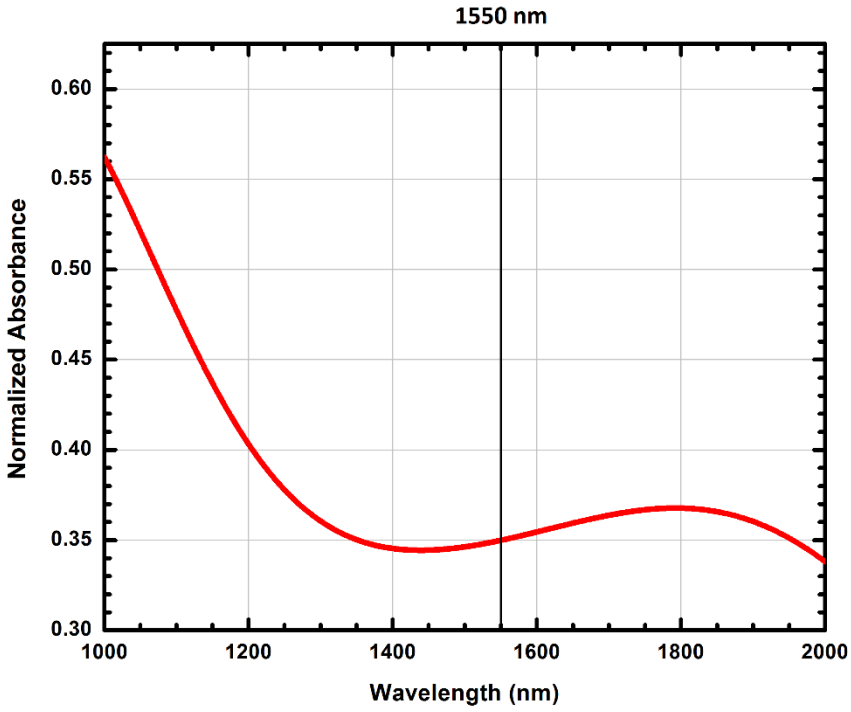

Fig. 5.26: Normalized Absorbance vs Wavelength.

Fig 5.26 shows the electric field distribution at the optical communication wavelength of 1550 nm. Field profile across the cross-sectional plane of the metal-dielectric-metal waveguide has been depicted on Fig 5.27. It is evident from Fig 5.26 that the electric field distribution is almost zero in the metallic region of the coupler.

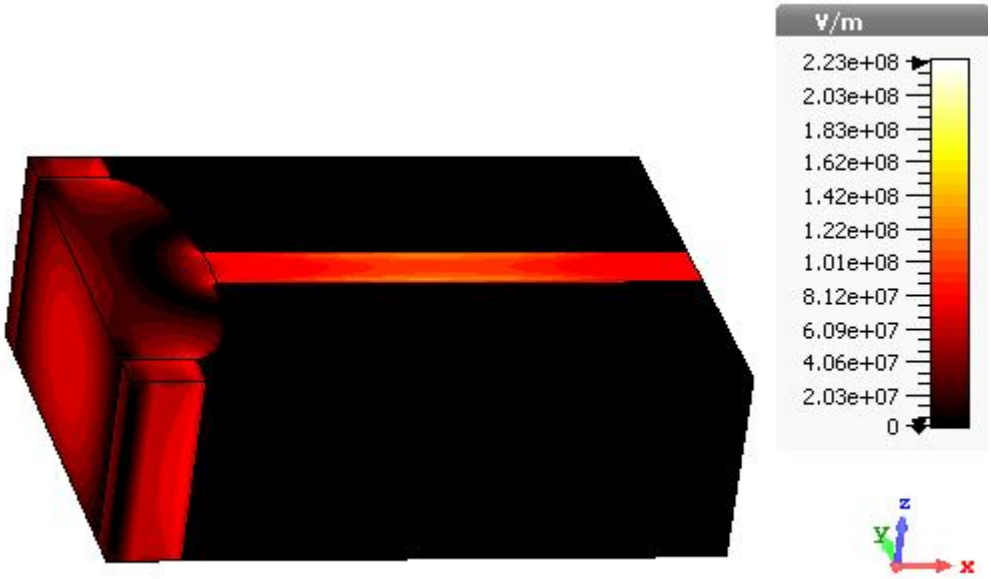

Fig. 5.27: Electric field distribution at 1550 nm.

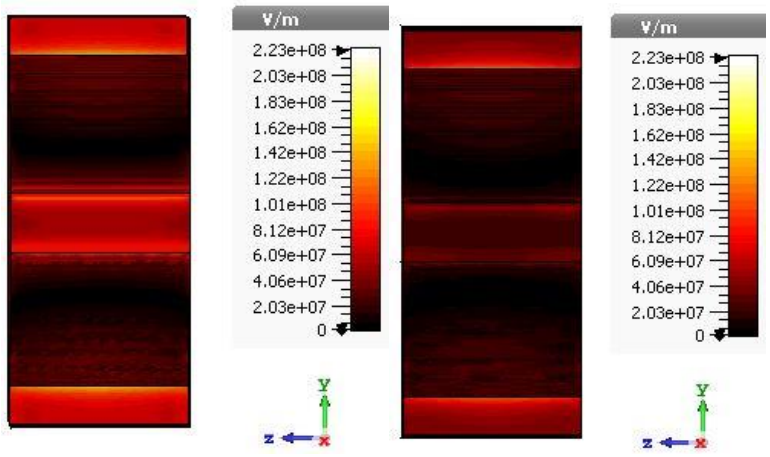

(a) (b)

Fig. 5.28: Cross-sectional view of electric field distribution at(a) 40 nm and (b) 120 nm away from the interface of dielectric and plasmonic waveguide.

Different performance specifications at the optical communication wavelength (1550 nm) have been inspected and are tabulated in Table 5.2.

Table 5.2: Values of different performance parameters at optical communication wavelength (1550 nm)

Sl. No.	**Parameters**	**Values**
1	Coupling Efficiency	63.169%
2	Reflectance	0.018
3	Absorbance	0.345

Chapter 6

Conclusion and Future Works

6.1 Conclusion

Plasmonic devices have progressed rapidly in recent years from isolated, passive structures to integrated active devices that could include an all-optical, nanophotonic networking application. The implementation of plasmonic nanostructures and extensive analysis of transmission properties have been theoretically demonstrated in this book. The accomplished work can be summarized as:

- Design and simulation of an efficient nano-plasmonic coupler by varying the dimension of certain parameters.
- Examining the change in performance characteristics of the coupler such as transmission efficiency, for different dimensional changes.
- Selection of an optimum structure for the proposed coupler which provides the most efficient result.

Throughout recent years, plasmonics has become an area of interest. Plasmonics are supposed to be the main nanotechnology integrating electronic and photonic elements on the same surface, in addition to creating modern photonics systems that are significantly smaller than the wavelength of the propagating light.

6.2 Future Works

The area of plasmonics provides multiple resources for study. These include plasmonic chips which serve as ultra-low-loss optical interconnections, super lenses that allow unparalleled optical imaging, and new sources of light with unprecedented quality deep-subwavelength nanolithography, plasmonic circuits and components that can direct light inside ultra-compact optically practical devices.

Following are the clearer view of what schemes lie ahead for upcoming days:

- Achieving a more appropriate architecture of the proposed model.
- Investigating the possibility of deploying new materials in order to achieve higher efficiencies.
- Effective monitoring of plasmonic stimuli by implementing piezoelectric modulation, all-optical and electro-optic and gain mechanisms to plasmonic structures.

Further work needs to be carried out in this particular field in order to satisfy the commitments made by plamonics. We also desire to have valuable contribution in this promising field by working on the modification of our proposed coupler.

References

[1] Ekmel Ozbay, "Plasmonics : Merging Photonics and," *Science (80-.).*, vol. 189, no. 2006, pp. 189–194, 2012.

[2] S. a. Maier, *Plasmonics: fundamentals and applications*. New york: Springer, 2004.

[3] D. K. Gramotnev and S. I. Bozhevolnyi, "Plasmonics beyond the diffraction limit," *Nat. Photonics*, vol. 4, no. 2, pp. 83–91, 2010.

[4] R. Zia, M. D. Selker, P. B. Catrysse, and M. L. Brongersma, "Geometries and materials for subwavelength surface plasmon modes," *J. Opt. Soc. Am. A*, vol. 21, no. 12, p. 2442, 2004.

[5] "Editorial: Surface plasmon resurrection," *Nat. Photonics*, vol. 6, no. 11, p. 707, 2012.

[6] M. Allione, V. V Temnov, Y. Fedutik, and U. Woggon, "Nl071763O.Pdf," 2008.

[7] G. Veronis and S. Fan, "Guided subwavelength plasmonic mode supported by a slot in a thin metal film," *Opt. Lett.*, vol. 30, no. 24, p. 3359, 2005.

[8] G. Veronis, W. Shin, and S. Fan, "Compact couplers between dielectric and metal-dielectric-metal plasmonic waveguides," *Opt. InfoBase Conf. Pap.*, vol. 15, no. 3, pp. 1158–1160, 2007.

[9] P. Ginzburg and M. Orenstein, "Plasmonic transmission lines: from micro to nano scale with λ/4 impedance matching," *Opt. Express*, vol. 15, no. 11, p. 6762, 2007.

[10] D. F. P. Pile *et al.*, "Two-dimensionally localized modes of a nanoscale gap plasmon waveguide," *Appl. Phys. Lett.*, vol. 87, no. 26, pp. 1–3, 2005.

[11] D. F. P. Pile and D. K. Gramotnev, "Adiabatic and nonadiabatic nanofocusing of plasmons by tapered gap plasmon waveguides," *Appl. Phys. Lett.*, vol. 89, no. 4, 2006.

[12] R. A. Wahsheh, Z. Lu, and M. A. G. Abushagur, "Integrated nanoplasmonic splitter," *2013 High Capacit. Opt. Networks Emerging/Enabling Technol. HONET-CNS 2013*, pp. 155–156, 2013.

[13] R. Wahsheh, "Nanoplasmonic Air-Slot Coupler: Design and Fabrication," *Front. Opt.*, 2012.

[14] S. M.N., *Elements of Electromeagnetics*. 2000.

[15] David M. Pozar, *Microwave Engineering*, $th. Wiley.

[16] R. Bansal, *Engineering Electromagnetics*. 2004.

[17] R. Marklein, "The Finite Integration Technique as a General Tool to Compute Acoustic , Electromagnetic , Elastodynamic , and Coupled Wave Fields," *Rev. Radio Sci. 1999-2002 URSI*, no. February, pp. 201–244, 2002.

[18] B. Jean-Pierre, “A perfectly matched layer for the absorption of electromagnetic waves,” *J. Comput. Phys.*, vol. 114, no. 2, pp. 185–200, 1994.

[19] Z. Rahimi, “The Finite Integration Technique (FIT) and the Application in Lithography Simulations,” p. 132, 2011.

[20] M. M. Mansour, M. El-Mala, A. A. T. Shalaby, E. S. M. El-Rabaie, and N. W. Messiha, “CRLH ZOR metametrial, design, simulation and fabrication,” *Proc. 2013 2nd Int. Japan-Egypt Conf. Electron. Commun. Comput. JEC-ECC 2013*, pp. 71–76, 2013.

[21] L. Liu, Z. Han, and S. He, “Novel surface plasmon waveguide for high integration,” *Opt. Express*, vol. 13, no. 17, p. 6645, 2005.

[22] M. G. Saber and R. H. Sagor, “Analysis of cuprous oxide-based ultra-compact nanoplasmonic coupler,” *Appl. Nanosci.*, vol. 5, no. 2, pp. 217–221, 2015.

[23] P. B. Johnson and R. W. Christy, “Optical-Constants Of Noble-Metals Phys. Rev. B 6(12), 4370–4379 (1972).,” *Phys. Rev. B*, vol. 1318, no. 1970, pp. 4370–4379, 1972.

[24] M. G. Saber and R. H. Sagor, “A comparative study of dielectric materials as nano-plasmonic couplers,” *2014 Int. Electr. Eng. Congr. iEECON 2014*, pp. 3–6, 2014.

[25] I. Munteanu and T. Weiland, “RF & Microwave Simulation with the Finite Integration Technique – From Component to System Design,” pp. 247–260, 2007.

[26] M. S. Islam Sumon, M. Tazwar, R. H. Sagor, and S. Mahtab Khandaker, “Design and analysis of a semi-elliptical ultra-compact nano-plasmonic coupler,” *1st Int. Conf. Robot. Electr. Signal Process. Tech. ICREST 2019*, pp. 417–421, 2019.